Cancer Nanotechnology

RESEARCH Open Access

Anticancer properties of copolymer nanoparticles loaded with *Foeniculum vulgare* derivatives in Hs578T and SUM159 cancer cell lines

Shima Bourang[1], Sodabeh Jahanbakhsh Godehkahriz[1*], Mehran Noruzpour[1], Rasool Asghari Zakaria[1] and Sergio Granados-Principal[2,3,4]

*Correspondence: jahanbakhsh@uma.ac.ir; soodabehjahanbakhsh@yahoo.com

[1] Department of Plant Production and Genetics, Faculty of Agriculture and Natural Resources, University of Mohaghegh Ardabili, Ardabil, Iran
[2] Department of Biochemistry and Molecular Biology 2, School of Pharmacy, University of Granada, 18011 Granada, Spain
[3] GENYO, Centre for Genomics and Oncological Research, Pfizer/University of Granada/Andalusian Regional Government, 18016 Granada, Spain
[4] Instituto de Investigación Biosanitaria ibs.GRANADA, University Hospitals of Granada-University of Granada, Conocimiento s/n, 18100 Granada, Spain

Abstract

Background: In recent years, the rising occurrence of cancer, particularly breast cancer, has led to a growing interest in utilizing nanotechnology for treatment. As a result of the significant side effects of chemical drugs, researchers have explored the potential of plants with antioxidant properties as an alternative option. *Foeniculum vulgare* is one of the potent plants for cancer therapy due to its rich anticancer compounds such as anethole, quercetin, kaempferol, and rutin found in its essential oil and ethanolic extract.

Methods: This study was conducted to investigate the antitumor properties of *F. vulgare*, along with the application of copolymers for their targeted delivery to Hs578T and SUM159 cancer cells. First, the ethanolic extract was derived from aerial parts and calluses of *F. vulgare* through the percolation technique, while the plant's essential oil extraction was carried out according to the Bettaieb et al method. Second, polymer nanoparticles composed of PLA–chitosan were synthesized, and their characteristics were investigated using various techniques such as Hydrogen nuclear magnetic resonance spectroscopy (^{1}H-NMR), Fourier transform infrared spectroscopy (FTIR), and thermogravimetric analysis. The preparation of PLA–PEG–HA/PLA–chitosan nanoparticles was accomplished via a solvent diffusion method and the physicochemical properties of these nanoparticles including their size, zeta potential, morphology, size distribution, and magnetic features were evaluated. The encapsulation efficiency of copolymers with *F. vulgare* ethanolic extract, essential oil, anethole, and pure quercetin was analyzed. After that, the drug release kinetics (at pH = 5 and 7.4), *in vitro* cytotoxicity evaluation, and analysis of cell apoptosis to evaluate the efficacy of drug delivery to Hs578T and SUM159 triple-negative breast cancer cell lines were evaluated.

Results: The results of the study indicated that PLA–PEG–HA/PLA–chitosan nanoparticles possess a spherical shape with an average size of 240 nm and a zeta potential of -10.8 mV. Moreover, the drug release pattern illustrated a higher release rate from synthesized nanoparticles under acidic conditions (pH = 5). The WST-1 assay revealed the biocompatibility of the drug-free nanocarriers and their minimal toxicity.

Additionally, the cell apoptosis results indicated a higher proportion of pre- and post-apoptotic cells in Hs578T cells compared to SUM-159 cells. Particularly, the Hs578T cell line treated with PLA–PEG–HA/chitosan–PLA/quercetin nanoparticles exhibited the highest percentages of pre- and post-apoptotic cells (34.06% and 8.19%, respectively).

Conclusions: The PLA–chitosan and PLA–PEG–HA/chitosan–PLA copolymer nanoparticles exhibit a noteworthy capacity for the targeted delivery of quercetin, anethole, and other anticancer compounds present in the ethanolic extract and essential oil of *F. vulgare* toward cancerous cells.

Keywords: Breast cancer, Encapsulation efficiency, Essential oil, Ethanolic extract, *F. vulgare*, Targeted drug delivery

Graphical Abstract

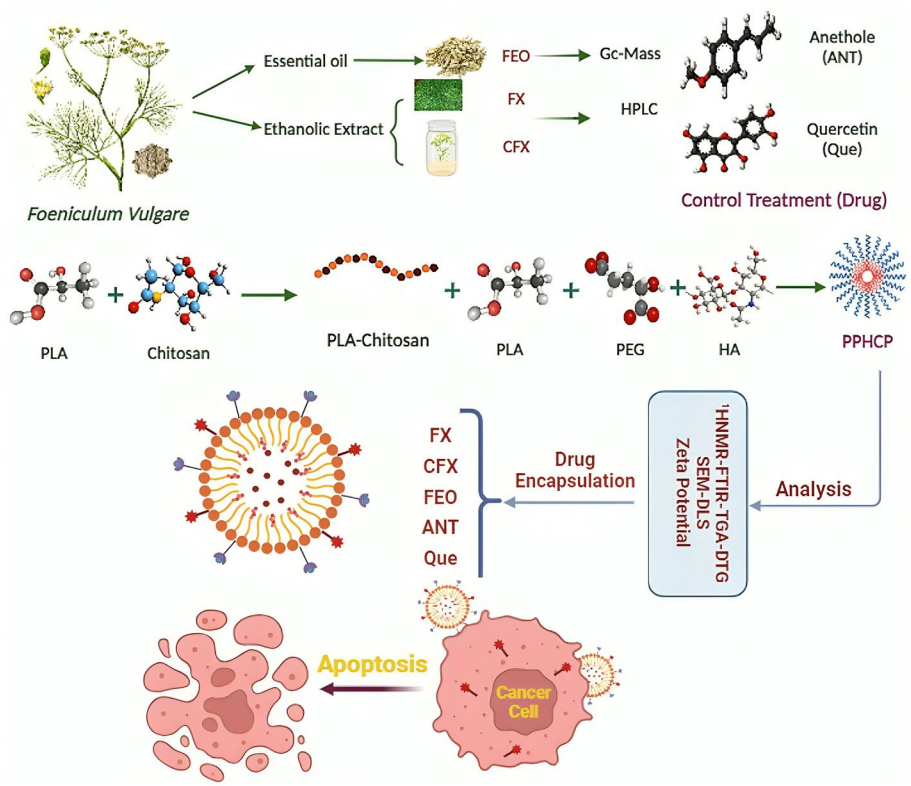

Introduction

Foeniculum vulgare Mill., a member of the Apiaceae family (Umbelliferaceae), has cytoprotective, hepatoprotective, antitumor, hypoglycemic, estrogenic, and antioxidant properties and is utilized globally for treating diverse health disorders, such as abdominal pain, arthritis, cancer, constipation, and insomnia (Rauf et al. 2022).

Phytochemicals such as phenols, alkaloids, terpenoids, flavonoids, glycosides, tannins, and saponins have been identified in the ethanol extract of *F. vulgare* seeds (Ghasemian et al. 2020). The main phenolic and flavonoid compounds in *F. vulgare*, rutin, quercetin, apigenin, ferulic acid, coumaric acid, and caffeic acid, are known to

have anti-inflammatory and antioxidant properties (Noreen et al. 2023). Moreover, *F. vulgare* seed essential oil contains α-pinene, fenchone, anethole, and estragole and has pharmacological effects, such as anti-inflammatory, antispasmodic, and antitumor effects (Kaur et al. 2022). Quercetin plays an important role in modulating the fundamental characteristics of cancer and signaling pathways associated with tumors (Reyes-Farias and Carrasco-Pozo 2019). It has been demonstrated to have anticancer effects on cancer cells through the regulation of key molecular components within signaling pathways, including PI3K/Akt/mTOR, Wnt/β-catenin, and MAPK/ERK1 (Rather and Bhagat 2020). Anethole, also known as trans-anethole, has been shown to inhibit the activation of NF-activated KBs by TNF transcription factors (Chainy et al. 2000). This inhibition of cellular responses induced by cytokines such as TNF sheds light on the potential cancer-preventive mechanisms of anethole (Akhbari et al. 2019).

Cancer is now recognized as one of the deadliest diseases in the world (Arnold et al. 2022). According to the 2023 GLOBOCAN global burden cancer analysis report, breast cancer (BC) has surpassed lung cancer as the most commonly diagnosed cancer among women (Organization and Breast cancer 2024). There are several methods of treatment according to pathological attributes such as surgery, radiation therapy, chemotherapy, targeted therapy, and immunotherapy (Smolarz et al. 2022). In some cases, the treatment plan may include a combination of treatment methods to maximize treatment effectiveness (Correia et al. 2021). Among them, chemotherapy is the most commonly used option to treat most cancers (Tang et al. 2024). Chemotherapy has the ability to eradicate numerous cancer cells throughout the body, eliminate tiny pockets of disease that surround the periphery of tumors evade a surgeon's observation, and can be used in conjunction with other therapeutic methods (Akbarzadeh et al. 2021).

In the field of drug design and development, various nanotechnologies are used to improve cancer treatment by eliminating inherent defects (Akbarzadeh et al. 2021). Collectively known as cancer nanotechnology, these nanotechnologies are being used to make drugs that are not only more effective therapeutically but also safer for the patient to use (Mosleh-Shirazi et al. 2022). However, the limited functionality of these drugs to dissolve in water and cross membranes has resulted in inadequate absorption in the body and reduced effectiveness of treatment (Pomeroy et al. 2022). Therefore, the use of nanoparticles to achieve controlled release and targeted delivery of these anticancer drugs is very important to improve therapeutic efficacy and reduce side effects associated with cancer treatments (Qiu et al. 2022). Nanotechnology has stimulated considerable interest in the development of novel pharmaceutical carriers and delivery systems (Alrushaid et al. 2023). Nanocarriers play a critical role in precisely delivering drug molecules to target sites, aiming to eradicate cancer cells while reducing adverse effects on healthy cells, thereby reducing the incidence of drug-related side effects (Yang et al. 2020). Varieties of nanoparticles used in targeted drug delivery include liposomes, polymeric nanoparticles, gold nanoparticles, silica nanoparticles, dendrimers, and solid lipid nanoparticles (Mosleh-Shirazi et al. 2022).

Polymeric nanoparticles (NPs), such as chitosan, human serum albumin (HSA), or bovine serum albumin (BSA), exhibit biocompatibility and biodegradability, thereby

assuming a significant function in the realm of therapeutic and receptor-mediated drug administration (Zhang et al. 2021).

Micelles are known for their spherical amphiphilic compositions, which typically range from 10 to 100 nm (Ibrahim et al. 2022a). Natural macromolecules or biocompatible synthetic polymers are used to create polymeric micelles (Gregoriou et al. 2021). Biodegradable polymers, such as polylactide (PLA), polyethylene glycol (PEG), chitosan, poly(DL-lactic-co-glycolic acid) (PLGA), and poly(ε-caprolactone) (PCL), have gained attention for biomedical applications because of their biocompatibility, degradability, and low toxicity (Junnuthula et al. 2022).

PLA is a thermoplastic, high-strength, high-modulus polymer derived through the fermentation of sustainable agricultural waste into carboxylic acid (Bourang et al. 2024a). The biodegradability and biocompatibility of PLA-based nano- and micro- particles have made them popular for safe adjuvant applications (Mundel et al. 2022). Its properties, such as mechanical strength and ease of processing, enable the development of various drug delivery forms, including nanoparticles, microspheres, and implants that can provide targeted or controlled drug release (Farkas et al. 2022). PLA's ability to degrade into non-toxic lactic acid makes it suitable for biomedical use, enhancing patient safety, and compliance by allowing for sustained release with less frequent dosing (Farkas et al. 2022; Khosraviboroujeni et al. 2022).

Chitosan is soluble through primary amine protonation in aqueous acidic media (Das et al. 2024). Its inherent qualities include non-toxicity, cationic nature, biocompatibility, and biodegradability (Tian and Liu 2023). Advantages of chitosan contribute to its potential use in drug delivery, biomedicine, and the development of nanocarrier systems (Al-Nemrawi et al. 2022). Compared with other natural polysaccharides, chitosan can deliver higher drug concentrations and form intermolecular crosslinks with multiple anions.

Polyethylene Glycol (PEG) is a versatile, hydrophilic polymer known for its biocompatibility and low immunogenicity, making it widely used in drug delivery systems (Shi et al. 2021). One of its key characteristics is its ability to form stable conjugates with various drugs, enhancing their solubility and stability (Ioele et al. 2022). PEG can modify the pharmacokinetics of therapeutic agents by extending their circulation time in the bloodstream, which helps achieve sustained and controlled release profiles (Tedeschini et al. 2021). Furthermore, its hydrophilic properties aid in reducing protein adsorption and prolonging clearance, which minimizes side effects while enhancing the drug's efficacy (Verma et al. 2024). The tunable molecular weight of PEG allows for customization of drug delivery systems, making it suitable for various formulations, including nanoparticles, hydrogels, and liposomes (Ibrahim et al. 2022b). Overall, PEG enhances the performance of drug delivery systems by improving drug solubility, reducing toxicity, and facilitating targeted delivery, ultimately leading to better therapeutic outcomes (Jin et al. 2017).

Despite the advantages of chitosan, PLA, and PEG in drug delivery systems, each has notable limitations that can affect their effectiveness. Chitosan, while biocompatible and biodegradable, has limited solubility at neutral pH, which can restrict its application for certain drugs and result in inconsistent drug release profiles (Herdiana et al. 2021). PLA's degradation rate can vary significantly based on environmental factors,

potentially leading to premature drug release or insufficient therapeutic levels over time; moreover, its hydrophobic nature makes it challenging to encapsulate hydrophilic drugs effectively (Shah et al. 2021). PEG, although beneficial for enhancing solubility and circulation time, may also lead to issues such as the "stealth effect," where PEGylation could mask drug activity or hinder cellular uptake if not properly designed (Levit and Tang 2021). Furthermore, the extensive use of PEG raises concerns about potential immunogenicity with repeated dosing. Together, these limitations highlight the need for ongoing research and development to optimize these materials and improve their functionality in drug delivery systems (Bholakant et al. 2021).

Pharmaceutical development and innovation are increasingly shifting towards a "smart drug" approach that prioritizes improved efficacy and reduced toxicity (Prajapati et al. 2024). This strategy focuses on delivering cancer chemotherapeutics directly to specific tumor receptors (Kalaydina et al. 2018). By identifying unique surface receptors on cancer cells, targeted delivery of chemotherapeutics and other therapeutic agents, such as small interfering RNA (siRNA), can significantly minimize side effects while enhancing the effectiveness of cancer treatments (Mirzaei et al. 2021).

In breast cancer, several markers present promising targets for precise drug delivery, including the overexpressed estrogen receptor (ER), progesterone receptor, HER2 receptor, folate receptor (FR), epidermal growth factor receptor (EGFR), transferrin receptor (TfR), integrin receptor, nucleoli receptor, and CD44 receptor (Saghaeidehkordi 2021). These receptors are significantly overexpressed on breast cancer cells compared to normal cells, providing an attractive approach for the delivery of potent anticancer agents through nanoparticulate systems, and partially overcome resistance mechanisms related to the active efflux of drugs from cancer cells.

Furthermore, hyaluronic acid (HA) is an essential component of the extracellular matrix and is widely used for anticancer drug delivery because of its biocompatibility, biodegradability, and non-toxicity, along with its non-immunogenic properties and multiple functional groups, such as carboxyl and hydroxyl sites for modification (Kiani-Dehkordi et al. 2023). Additionally, HA acts as a natural ligand in targeted drug delivery systems due to its interaction with the endocytic receptor CD44, which is often overexpressed in various cancer cells (Rios de la Rosa et al. 2018). Consequently, HA-based nanocarriers have been engineered to enhance drug delivery efficiency while effectively distinguishing between healthy and cancerous tissues, ultimately minimizing residual toxicity and off-target effects (Della Sala et al. 2022).

In recent years, interest in the use of herbal compounds as alternatives to traditional chemotherapy drugs has increased (Wangchuk 2018). This shift in focus can be attributed to the high side effects associated with chemotherapy drugs, as well as their detrimental impact on healthy cells within the body (Esmeeta et al. 2022). In this study, following the synthesis of polymeric nanoparticles utilizing PLA–PEG–HA/chitosan–PLA, we investigated the effects of these nanoparticles on the targeted delivery of pure quercetin, pure anethole, anticancer compounds from the ethanol extract of *F. vulgare* (aerial parts and selected callus tissue), and essential oils for regulating the growth and viability of Hs578T and SUM159 triple-negative breast cancer cell lines.

Materials and methods

Plant material and explant source (in vivo production)

The aerial parts (newly grown stems) of *F. vulgare* used as explants to produce callus tissue *in vitro* were collected from the Medicinal Plants Research Center at Ardabil University of Medical Sciences. After surface disinfection, the explants were cultured in Murashige and Skoog medium (MS) media supplemented with 2 mg/L NAA (1-naphthalene acetic acid) and 0.5 mg/L Kin (kinetin).

After that, the callus samples were subjected to three consecutive subcultures to maintain genetic purity. The calluses were subsequently treated with different concentrations of plant growth stimulants—methyl jasmonate, salicylic acid, and phenylalanine—at zero (control), 50, 100, and 200 mg/L for 24, 48, and 96 h. In this study, the callus sample grown in media supplemented with 200 mg/L methyl jasmonate for 96 hours presented the greatest accumulation of secondary metabolites. As a result, this specific callus was selected for further extraction procedures (Bourang et al. 2024b).

Extraction of essential oils from *F. vulgare* seeds

The mature *F. vulgare* seeds used in this study were purchased from the Seed and Plant Improvement Institute (SPII) in Iran. Essential oil was extracted from the *F. vulgare* seeds via hydrodistillation with a Clevenger apparatus, following the method outlined by Bettaieb et al. (2011). After extraction, the oil was dried with anhydrous sodium sulfate, filtered, and stored at 4 °C for use in tests and evaluations.

Identification and quantification of the essential oil components

Analysis of the *F. vulgare* essential oil was performed via gas chromatography–mass spectrometry (GC–MS, Agilent 7890B series GC–MS). Components were identified by comparing their mass spectra with the Wiley Registry 9th Edition/NIST 2011 mass spectral library and their retention indices with those of authentic compounds or literature values. The relative percentage of these components was calculated by electronically integrating peak areas without applying a correction factor.

Extraction of the ethanolic extract

The extraction process was carried out at Mohaghegh Ardabili University Biotechnology Laboratory via double-distilled water, the Percolation method, and a 15:1 sample to 70% ethanol solvent ratio (for leaf and callus samples) to extract quercetin. In this procedure, 15 ml of 70% ethanol was mixed with 1 g of plant material (dried leaf or callus) (Lutviani et al. 2023). The resulting mixture was filtered and centrifuged at 4000 rpm, and the upper layer was collected as the final plant extract for testing. Additionally, a control sample of quercetin powder was sourced from Sigma-Aldrich (Aldrich-337951).

HPLC analysis

Hurst et al. used high-performance liquid chromatography (HPLC) in 1983 (Hurst et al. 1983) to measure the levels of secondary metabolites of quercetin. An HPLC system (KENUVER, AZURA, Germany) with a C18 reversed-phase column was used

to analyze quercetin compounds in the supernatant from the leaf and callus tissues. The mobile phase consisted of HPLC-grade methanol and distilled water. Quercetin was detected and quantified at a wavelength of 368 nm. Pure quercetin samples (Sigma-Aldrich) at concentrations of 10, 20, 50, 100, and 500 mg/L were used to construct the standard curve.

Preparation of micellar nanoparticles

Synthesis of PLA–chitosan

Four grams of acrylate-PLA was dissolved in 20 ml of chloroform. Next, 4 g of chitosan was added to the solution and stirred for 24 h at 50 °C. The resulting mixture was then retrieved by replacing the solvents with methanol and water, followed by dialysis against water (with a molecular weight cutoff of 10,000) for two days at 4 °C to remove impurities (Parveen and Sahoo 2011).

Preparation of encapsulated nanoparticles

For this purpose, the method of Parveen and Sahoo (2011) was employed with slight modifications. Initially, 2 ml of each substance (including the ethanolic extract of *F. vulgare* plants (FX), ethanolic extract from the designated callus sample (CFX), essential oil of *F. vulgare* (FEO), and pure samples (trans-anethole (ANT) (Sigma-Aldrich) and quercetin (Que) (Sigma-Aldrich)) were combined with 2 ml of chloroform containing 50 mg of chitosan–PLA copolymer, incubated for 30 seconds on ice, and further sonicated. Next, the resulting solution was emulsified in 3 ml of water with the addition of 0.3% (w/v) polyvinyl alcohol (PVA) under sonication for two minutes. The chloroform in the mixture was evaporated, and the resulting nanoparticles were collected, washed with 100 ml of phosphate buffer, and centrifuged at 12000 rpm for thirty minutes. Subsequently, 10 ml of phosphate buffer was mixed with the nanoparticles, which were then filtered through a 0.45 μm membrane filter to remove larger nanoparticles. Finally, the nanoparticles were dried via a freeze dryer and stored at − 80 °C.

The formulations of the PLA–PEG–HA/chitosan–PLA nanoparticles incorporating *F. vulgare* extract (PPHCP/FX), the PLA–PEG–HA/chitosan–PLA nanoparticles containing an ethanolic extract from the callus (PPHCP/CFX), the PLA–PEG–HA/chitosan–PLA including *F. vulgare* essential oil (PPHCP/FEO), the PLA–PEG–HA/chitosan–PLA encapsulating pure trans-anethole (PPHCP/ANT), and the PLA–PEG–HA/chitosan–PLA encapsulating pure quercetin (PPHCP/Que) were developed following the same procedure, except that in addition to the chitosan–PLA copolymer, 50 mg of the PLA–PEG–HA copolymer was also included in 2 ml of chloroform (Fig. 1).

Characterization of the micelles

After the synthesis process, the nanoparticles were analyzed in detail via techniques such as hydrogen nuclear magnetic resonance spectroscopy (^{1}H-NMR-Bruker 400 MHz) and Fourier transform infrared spectroscopy (FTIR ABB Bomem MB). The characteristics, including morphology, size, zeta potential, and hydrodynamic diameter of the micelles, were assessed via advanced tools such as scanning electron microscopy (SEM, LEO 1430, Oberkochen, Zeiss), a zeta potential analyzer (SZ-100 Horiba), and dynamic light scattering (DLS, Malvern Instruments). Additionally, the thermal behaviors of PLA,

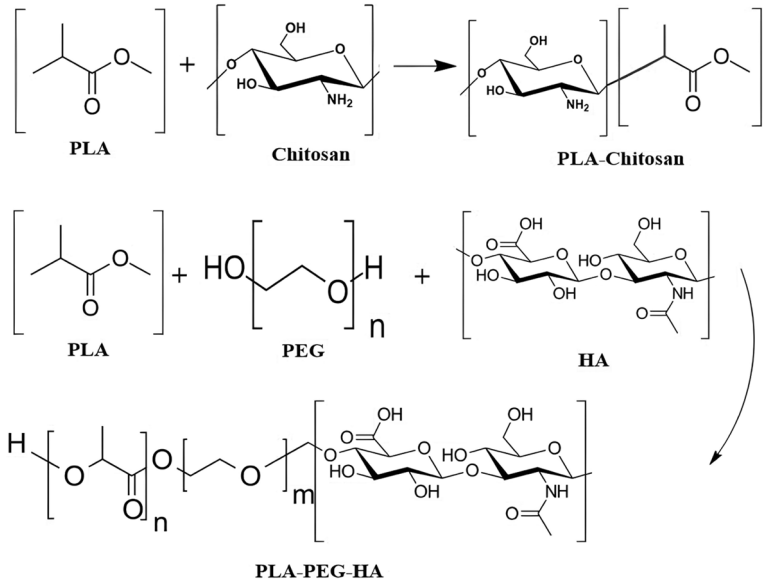

Fig. 1 Chemical scheme of PLA–chitosan and PLA–PEG–HA copolymer synthesis

chitosan, and PLA–chitosan were studied through thermogravimetric analysis (TGA) and a thermogravimetric derivative (DTG) (TG-DTA-32, Japan) in the temperature range of 25 °C to 600 °C with a heating rate of 20 °C/min under atmospheric air pressure.

Encapsulation efficiency

To calculate the encapsulation efficiency (EE) of FX, CFX, FEO, ANT, and Que in chitosan–PLA and PLA–PEG–HA/chitosan–PLA nanoparticles, a centrifugation step was first performed at 13,000 rpm for 1 hour to precipitate the synthesized nanoparticles from the previous step. Subsequently, the amount of unencapsulated FX, CFX, FEO, ANT, and Que in the supernatant of each sample was determined using a spectrophotometer (FX, CFX, and Que at a wavelength of 368 nm, and FEO and ANT at 260 nm). Finally, the obtained values were compared with the initial amounts of FX, CFX, FEO, ANT, and Que used in the encapsulation process (Bourang et al. 2024a).

Encapsulation efficiency of Que, FX, and CFX (wavelength: 368 nm):

$$\left(\mathrm{EE}_{\substack{\mathrm{Fx}\\ \mathrm{CFX}\\ \mathrm{Que}}}\ \%\right) = \left(\mathrm{W}_{\mathrm{initial}\,\substack{\mathrm{Fx}\\ \mathrm{CFX}\\ \mathrm{Que}}} - \mathrm{W}_{\mathrm{free}\,\substack{\mathrm{Fx}\\ \mathrm{CFX}\\ \mathrm{Que}}} \div \mathrm{W}_{\mathrm{initial}\,\substack{\mathrm{Fx}\\ \mathrm{CFX}\\ \mathrm{Que}}}\right) \times 100$$

Encapsulation efficiency of FEO and ANT (wavelength: 260 nm):

$$\left(\mathrm{EE}_{\substack{\mathrm{FEO}\\ \mathrm{ANT}}}\ \%\right) = \left(\mathrm{W}_{\mathrm{initial}\,\substack{\mathrm{FEO}\\ \mathrm{ANT}}} - \mathrm{W}_{\mathrm{free}\,\substack{\mathrm{FEO}\\ \mathrm{ANT}}} \div \mathrm{W}_{\mathrm{initial}\,\substack{\mathrm{FEO}\\ \mathrm{ANT}}}\right) \times 100.$$

Release patterns of the nanoparticles

Previous studies have shown that tumor tissue has a lower pH than normal tissue does (Nguyen et al. 2021; Chandrasekhar et al. 2020). This study aimed to replicate the drug release patterns from nanoparticles in both normal and cancerous tissues. The release

profiles of FX, CFX, FEO, ANT, and Que from various types of nanoparticles were examined in PBS buffer solutions with different pH values (pH=5 and pH=7.4). To accomplish this, 10 mg of each nanoparticle mixture was added to 2 ml of PBS buffer at various pH values. The supernatant containing the nanoparticles was then separated via centrifugation (13,000 rpm for 10 min), and the concentrations of the compounds in the supernatant were measured via a spectrophotometric device (Bio-Rad, SmartspecTM plus, United States of America) at specific wavelengths (368 nm for Que and 260 nm for ANT). After centrifugation, the sediment from the nanoparticles was resuspended in 2 ml of fresh PBS and placed in an incubator at 37 °C. The release percentages of the ethanolic extract and drug were calculated via the following equation:

$$\text{Release pattern of each nanoparticle (pH } 5, 7.4) : \frac{Dr_t + Dr_{t+1}}{DE},$$

Dr_t, The measured amount of drug in the supernatant at any time (t); Dr_{t+1}, The measured amount of drug in the supernatant at time t+1; De, The amount of drug encapsulated in the nanoparticles.

Cell culture

The triple-negative breast cancer cell lines Hs578T and SUM159 were obtained from the ATCC and Asterand, respectively. Both cell lines were cultured in DMEM (Dulbecco's modified Eagle's medium, Sigma-Aldrich) supplemented with 10% FBS (fetal bovine serum, Thermo Fisher Scientific) at 37°C and 5% CO_2 as previously described (Calahorra et al. 2024).

In vitro evaluation of cytotoxicity

The concentration at which each drug demonstrated half of its maximal inhibitory effect on tumor cell viability (IC_{50}) was assessed via the WST-1 assay with a Nanoquant plate reader (Tecan). For this aim, Hs578t and SUM159 cells were seeded into 96-well tissue culture plates at the concentrations of 5×10^3 and 2×10^3 cells/well, respectively, and incubated for 24 h. After, the cell lines were separately treated with different concentrations (0, 5, 10, 25, 50 µg/ml) of nanoparticles (CP/FX), (CP/CFX), (CP/Que), (CP/FEO), (CP/ANT), (PPPHCP/FCPFX), (PPPHCP/FCPFX), (PPHCP/FEO), and (PPHCP/ANT), as well as concentrations of free compounds without nanoparticles (0, 5, 10, 25, 50 µl/ml) of FX, CFX, FEO, ANT, and Que for 24 h.

To assess the impact of nanoparticles on the transfer efficiency of FX, CFX, FEO, ANT, and Que, the quantity of nanoparticles used for treating Hs578T and SUM159 cells was calculated to ensure that the treatments included equivalent amounts of the specified compounds. WST-1 reagent (Roche) was added to each well, and the absorbance of the samples of interest at a wavelength of 440 nm was measured by a Nanoquant plate reader at 10, 15, 30, and 45 min and compared with that of the control treatment (no treatment) (Calahorra et al. 2024).

Cell apoptosis analysis

Apoptosis was assayed by flow cytometry with an Annexin V-FITC apoptosis kit (BestBio) in Hs578T and SUM159 cells treated with FX, CFX, FEO, ANT, Que, and

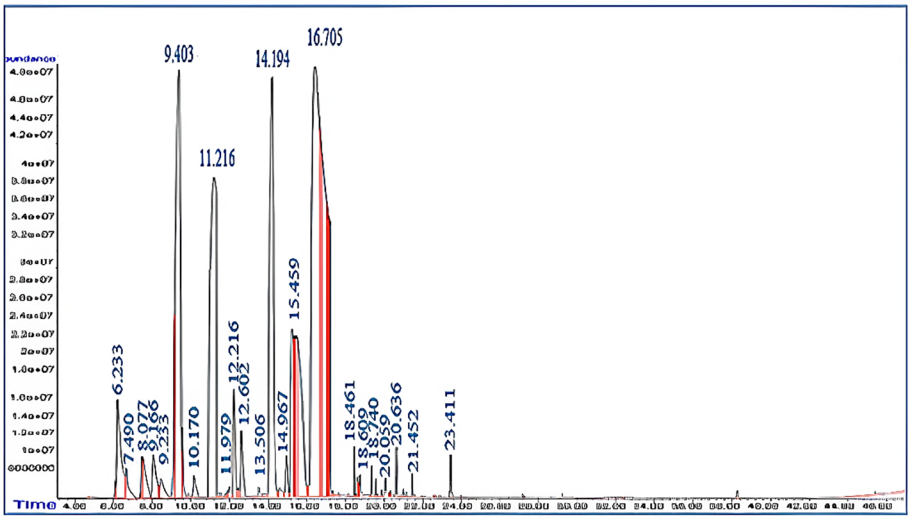

Fig. 2 GC–MS chromatogram results of *F. vulgare* essential oil, taken from two stages of gas chromatography and mass spectrometry. In this diagram, molecular structures are identified and determined, and after interpretation of the results, the desired compound is reported

encapsulated nanoparticles [(CP/FX), (CP/CFX), (CP/Que), (CP/FEO), (CP/ANT), (PPHCP/FX), (PPHCP/CFX), (PPHCP/Que), (PPHCP/FEO), and (PPHCP/ANT)] for 48 h. In accordance with the manufacturer's instructions, the cells were stained with Annexin V and propidium iodide (PI) for 15 minutes at room temperature in the dark (Dávila-González et al. 2018). Flow cytometric analysis was performed using a BD Accuri C6 instrument, and data analysis was carried out with FlowJo software version 10.

Results

GC–MS analysis of *F. vulgare* essential oil

The results of the GC–mass analysis of the essential oil of *F. vulgare* (Fig. 2 and Table 1) revealed the presence of flavonoid compounds, such as sabinene, estragole, beta-pinene, apiol, limonene, and alpha-phellandrene, L-fenchone, and anethole, are associated with anti-inflammatory, antibacterial, antioxidant, antidiabetic, and anticancer properties.

HPLC analysis

Rutin, quercetin, and kaempferol levels in the ethanolic extracts of *F. vulgare* plants and callus tissue were quantified via HPLC and analyzed (Table 2).

Characterization of the micelles

Proton nuclear magnetic resonance (^{1}H NMR)

In this research, ^{1}H-NMR spectroscopy was used to confirm the synthesis of the PLA–chitosan–HA polymer. Signals related to methylene carbonyl groups (CH_2-CO) were recorded in the range of 5.3–5.6, and methyl signals (CH_3) were recorded in the range of 1.4–1.7 for PLA. After the attachment of chitosan to PLA, signals related to the methine

Table 1 Results of GC–mass analysis of the essential oil of *F. vulgare*

Compounds	Molecular formula	Retention Time	Total (%)	Recorded pharmacological activity	References
(1*R*)-(+)-α-Pinen	$C_{10}H_{16}$	6. 233	2.631	–	–
4-Carene	$C_{10}H_{16}$	6. 678	0.617	–	–
beta-phellandrene	$C_{10}H_{16}$	7. 490	0.369	–	–
Sabinene	$C_{10}H_{16}$	7. 544	0.884	Anti-inflammatory	Lima et al. (2016)
beta-pinene	$C_{10}H_{16}$	8. 077	1.038	Antibacterial	Lima et al. (2016)
alpha-phellandrene	$C_{10}H_{16}$	8. 460	0.512	Antibacterial	Boevé et al. (2023)
D-Limonene	$C_{10}H_{16}$	9. 403	12.291	Antibacterial, antifungal, and antitumor	Bai et al. (2016)
3-Carene	$C_{10}H_{16}$	9. 565	0.583	Antibacterial, antioxidant, and anticancer	Shu et al. (2020)
1,4-Cyclohexadiene, 1-methyl-	C_7H_{10}	10. 170	0.380	–	–
L-Fenchone	$C_{10}H_{16}O$	11. 216	12.234	Anti-inflammatory, antioxidant, antidiarrheal, antifungal, antinociceptive, and bronchodilator	Kang et al. (2019)
Bicyclo [2. 2. 1]heptane containing *N,N′*-diarylsquaramide	$C_{10}H_{16}$	11. 979	0.136	Anticancer, antiviral, and antibacterial	Kang et al. (2019)
2,6-Dimethyl-2,4,6-octatriene	$C_{10}H_{16}$	12. 216	1.377	–	–
Bicyclo [2. 2. 1] heptan-2-one, 1,7,7-trimethyl-	$C_{10}H_{16}O$	12. 602	1.020	–	–
3-Cyclohexen-1-ol, 4-methyl-1-(1-methylethyl)-	$C_{10}H_{18}O$	13. 506	0.136	–	–
Estragole	$C_{10}H_{12}O$	14. 197	10.778	Antimicrobial, antioxidant, anticonvulsant, and macrophage	Roy et al. (2018)
Bicyclo [2. 2. 1] heptan-2-ol, 2-ethyl-1,3,3-trimethyl-	$C_{12}H_{12}O$	14. 969	0.569	–	–
2-Cyclohexen-1-one, 2-methyl-5-(1-methylethyl)-	$C_{10}H_{16}O$	15. 459	9.156	–	–
Anethole	$C_{10}H_{12}O$	16.705	35.194	Antifungal, antibacterial, analgesic, anti-inflammatory and antioxidant	Nasır and Yabalak (2021)
Copaene	$C_{15}H_{24}$	18.461	0.218	Antibacterial and anti-inflammatory	Kang et al. (2019)
2-Propanone, 1-(4-methoxyphenyl)-	$C_{10}H_{12}O$	18.609	0.133	–	–

Table 1 (continued)

Compounds	Molecular formula	Retention Time	Total (%)	Recorded pharmacological activity	References
1H-Cyclopenta[1,3] cyclopropa[1,2] benzene	$C_{15}H_{24}$	18.740	0.186	–	–
Bicyclo [4. 4. 0] dec-1-ene, 2-iso-propyl-5-methyl-9-methylene-	$C_{15}H_{24}$	19.354	0.172	–	–
Tricyclo [3. 3. 1. $1^{3,7}$] decane, tricyclo [3. 3. 1. $1^{3,7}$] decylidene-	$C_{20}H_{28}$	20.059	0.186	–	–
Tricyclo [3. 3. 1. $1^{3,7}$] decane, tricyclo [3. 3. 1. $1^{3,7}$] decylidene-	$C_{20}H_{28}$	20.636	0.240	–	–
Naphthalene, 1,2,3,5,6,8a-hexahydro-4,7-dimethyl-1-(1-methylethyl)-	$C_{15}H_{24}$	21.452	0.105	–	–
Apiol	$C_{12}H_{14}O_4$	23.411	0.255	Antioxidant, antifungal, anticancer, abortifacient, acaricidal, phytotoxic, antitumor, and antiproliferative agents	Kang et al. (2019)

polysaccharide (CH) of chitosan were observed in the range of 3.6 ppm, and amine protons (NH_2) were observed in the range of 2.8 ppm (Fig. 3A).

After the binding of hyaluronic acid, the protons in the glucuronic acid ring were detected in the range of 2.3–4.2 ppm. In addition, the protons of the N-acetyl glucosamine units and the protons attached to the amide groups in the N-acetyl group produced a peak at approximately 1.9 ppm (due to the methyl-acyl group), which confirmed the binding of hyaluronic acid to PLA–chitosan (Fig. 3B).

Fourier Transform Infrared Spectroscopy (FTIR)

The results of the FTIR spectroscopy of chitosan revealed that the peaks in the ranges of 1500–1600 cm^{-1} and 3200–3500 cm^{-1} are related to N–H and O–H bonds. The tension related to the C-O functional groups in the chitosan structure was also observed in the range of 1020–1150 cm^{-1} (Fig. 4A). Furthermore, according to the FTIR results for PLA (Fig. 4B), the peaks in the ranges of 1000–1500 cm^{-1} and 1500–2000 cm^{-1} correspond to C–O and C = O bonds, respectively. After chitosan was attached to PLA, the tension of the carbonyl group (C=O) changed slightly due to the interactions between PLA and chitosan but remained in the range of 1800–1700 cm^{-1} (Fig. 4C). Moreover, peaks related to N–H and O–H functional groups were observed in the ranges of 1500–1600 and 3200–3500 cm^{-1}. The peak observed in the 1100 region was attributed to the C–O–C group, which indicates the interaction between the saccharide structure of chitosan and PLA. The change in the position of some peaks as well as the changes in their

Table 2 Amounts of rutin, quercetin, and kaempferol in the ethanolic extracts of the shoot and callus tissues of *F. vulgare*

Compounds	Rutin ($mg.g^{-1}$)	Quercetin ($mg.g^{-1}$)	Kaempferol ($mg.g^{-1}$)
Amount in ethanolic extract of the plant shoot	27.92	18.78	10.15
Amount in ethanolic extract of the callus tissue	19.12	8.07	5.83

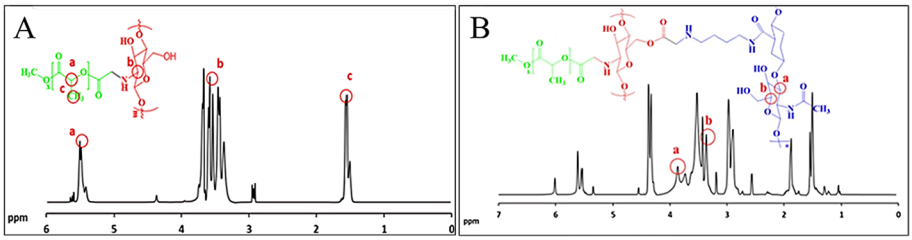

Fig. 3 ^{1}H-NMR spectroscopic analysis diagram of **a** PLA–chitosan and **b** PLA–chitosan–HA. The vertical axis is (intensity) and the horizontal axis is (multiplicity). Each peak in this spectrum refers to a specific type of proton in the molecule. The height and area of the peaks are related to the number and type of protons present in their specific chemical environment

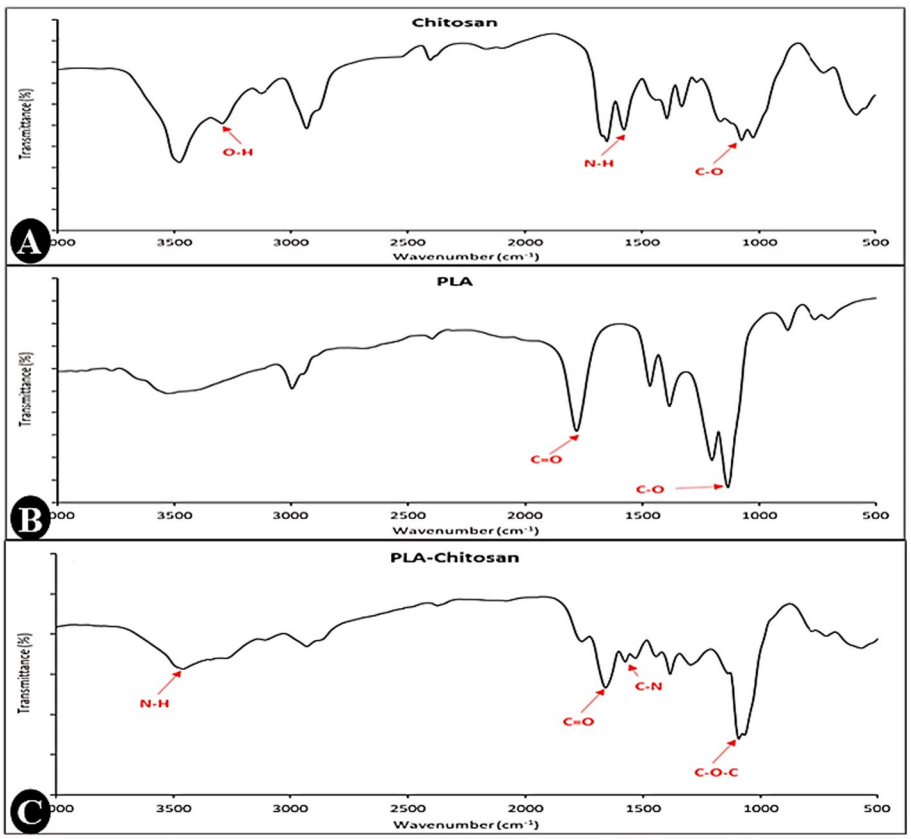

Fig. 4 FTIR spectra of **a** chitosan, **b** PLA and **c** PLA–chitosan. Horizontal axis (wavelength axis or wave number) and vertical axis (absorption intensity axis). In this spectrum, the absorption peaks indicate which functional groups are present in the sample under investigation

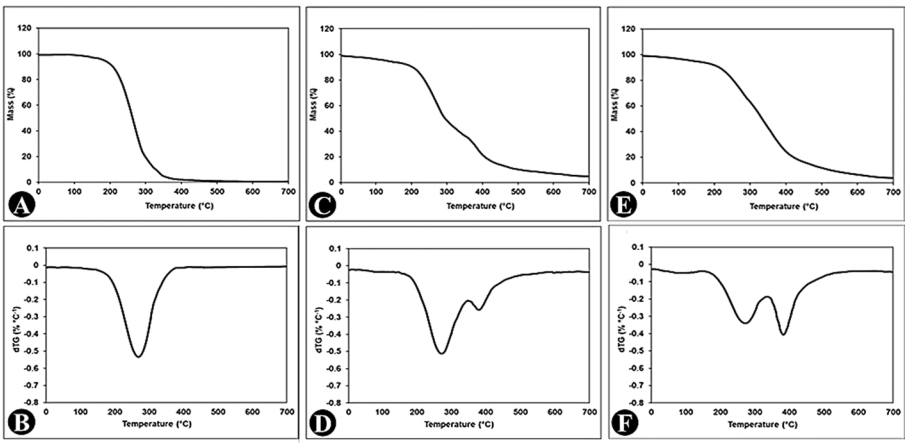

Fig. 5 TGA analysis of **A** PLA, **C** PLA–chitosan, and **E** PLA–chitosan–HA nanoparticles and DTG analysis of **B** PLA, **D** PLA–chitosan, and **F** PLA–chitosan–HA nanoparticles. The TGA curve shows the weight changes of the sample during increasing temperature or time. The DTG curve is the first derivative of the TGA curve and relates the rate of weight change to time or temperature. The shape of the DTG curve shows the peak points and the maximum rate of weight change, which can accurately identify the starting and ending points of material decomposition and thermal reactions

intensity can be caused by the interaction of PLA and chitosan, which indicates the correct synthesis of PLA–chitosan.

Thermal Gravitational Analysis (TGA) and Differential Thermal Gravitational Analysis (DTG)

The TGA diagram illustrates the decrease in the weight of the nanoparticles compared with the increase in temperature, and the DTG diagram demonstrates the rate of change in the rate of weight loss compared with the increase in temperature. According to the results of the TGA analysis of the PLA polymer, a weight loss stage at an approximate temperature of 250–300 °C was observed, which could be due to the chemical decomposition of the PLA polymer chains (Fig. 5A). In the DTG diagram of PLA, these points appear with sharp peaks, which indicates the high rate of decomposition of PLA at these temperatures (at 250 °C) (Fig. 5B).

By combining PLA and chitosan, the thermal decomposition behavior of PLA–chitosan in the TGA and DTA tests was affected by the presence of both PLA and chitosan. Therefore, the process of weight loss in the PLA–chitosan polymer was greater than that in the PLA. Furthermore, a trend toward temperature reduction was observed at a higher temperature than that of PLA and approximately 400 °C, which showed that chitosan is more resistant to temperature than is PLA (Fig. 5C). The DTG results revealed two peaks of weight loss in the ranges of 250 °C and 400 °C, indicating the presence of at least two main degradation stages, which probably corresponded to the degradation of the PLA and chitosan components at different temperatures (Fig. 5D).

In the PLA–chitosan–HA sample, the pattern of weight loss (TGA) changed so that the speed of weight loss in the PLA–chitosan–HA polymer at a temperature range of 400 °C was greater than that of the PLA–chitosan polymer (Fig. 5E). Additionally, the binding of hyaluronic acid to PLA–chitosan changed the DTG pattern (Fig. 5F), which indicated the binding of a new molecule to the PLA–chitosan compound.

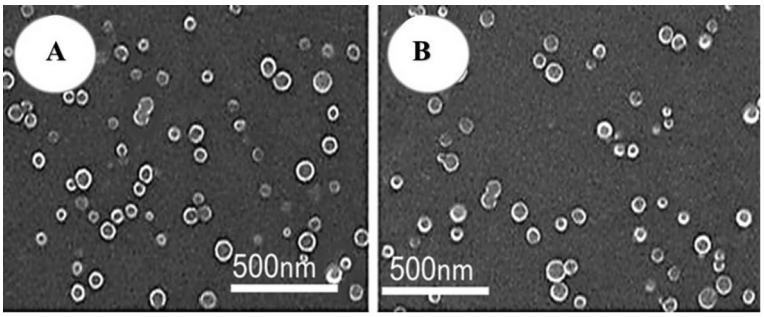

Fig. 6 SEM images of **a** PLA–chitosan/FX and **b** PPCPF/FX nanoparticles. The results include path plot and covariance matrix

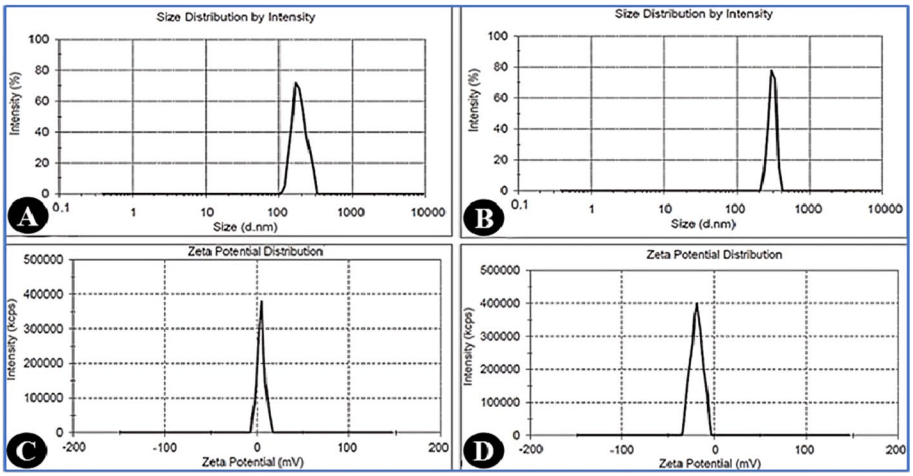

Fig. 7 DLS and zeta potential plots of; **a**, **b** size distribution of PLA/chitosan/FX and PPHCP/FX respectively and **c**, **d** zeta potential of PLA/chitosan/FX and PPCPF/FX. DLS results show the particle size distribution. Zeta potential provides information about the surface electric charge of the particles

Scanning electron microscopy (SEM) images of the PLA–chitosan/FX and PPCPF/FX nanoparticles

According to the results obtained from the SEM images, the PLA–chitosan/FX and PPHCP/FX nanoparticles are composed of relatively uniform geometric shapes with similar sizes (Fig. 6). These nanoparticles have smooth surfaces and clear boundaries, which indicate high purity and good control in the synthesis process. No significant differences in the size or morphology of the PLA–chitosan/FX and PPHCP/FX nanoparticles were observed. In both images (Fig. 6), the nanoparticles show good stability and lack the tendency to form large aggregates, which can be used in medical applications.

Dynamic light scattering (DLS) and graphical distribution of the zeta potential of the PLA–chitosan/FX and PPCPF/FX nanoparticles

The results obtained from the DLS diagram demonstrate the size distributions of the two PLA/chitosan/FX and PPHCP/FX nanoparticles (Fig. 7A, B). The resulting DLS diagram of the PLA/chitosan/FX nanoparticles revealed a peak with a suitable amplitude, which indicates the uniformity between the nanoparticles. The size of these nanoparticles was approximately 240 nm (Fig. 7A), and the DLS results of the PPHCP/FX nanoparticles

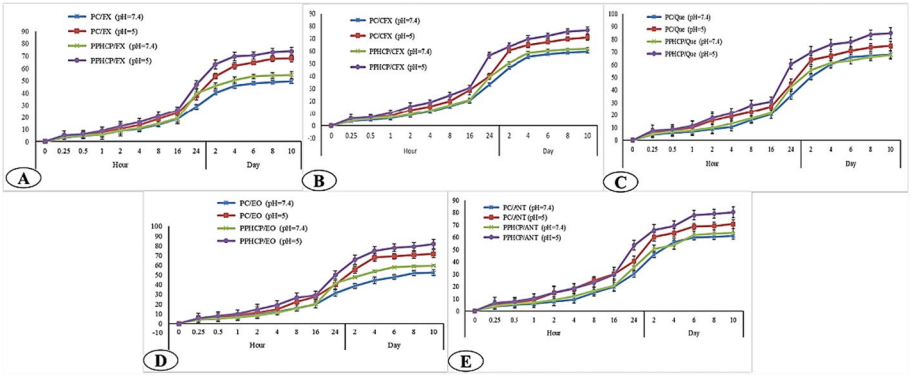

Fig. 8 Drug release patterns: **A** ethanolic extract of *F. vulgare* (FX), **B** ethanolic extract of selected callus tissue sample (CFX), **C** quercetin, **D** essential oil of *F. vulgare* (EO), and **E** anethole encapsulated in PLA–chitosan (CP) and PLA–PEG–HA/PLA–chitosan (PPHCP) nanoparticles at two different pH values (pH=7.4 and 5). Accurate and comprehensive analysis of drug release patterns will not only help in better understanding the performance of drugs but also in designing new formulations and optimizing treatments based on patient needs

revealed that their size was approximately 350 nm. The sharp peak in the DLS diagram of the resulting nanoparticle (Fig. 7B) suggested that the nanoparticles were uniform in size, which is usually favorable for uniform biological behavior and targeted drug delivery applications. The results of both graphs indicated that the preparation method of the nanoparticles in this research was appropriate and produced nanoparticles with the appropriate size and uniform distribution.

The graphical distribution of the zeta potential indicates the electrostatic stability of the nanoparticles. The zeta potential of the PLA/chitosan/FX nanoparticles demonstrated that they have an average positive charge (+8.7 mV) (Fig. 7C), and the PPHCP/FX nanoparticles had a negative zeta potential (− 10.8 mV) (Fig. 7D). The positive potential of nanoparticles is also important for biological interactions because positively charged nanoparticles can have better interactions with negatively charged biological membranes and improve cell uptake.

Drug release pattern

Figure 8 shows the release diagram of the ethanolic extract of *F. vulgare* plants (FX), ethanolic extract from a selected callus tissue sample (CFX), essential oil (EO), pure anethole (ANT), and pure quercetin (Que) from PLA–chitosan and PPHCP nanoparticles at acidic (pH = 5) and neutral (pH = 7.4) pH values. The evaluation of drug release continued until the cumulative concentration of the released compounds did not change. According to our results, the release rate of the active substances (FX, CFX, EO, ANT, and Que) increased at acidic pH values (pH=5). In addition, in both environments (pH = 7.4 and 5), the release rate of the effective substance from the PPHCP nanoparticles was higher than that from the PLA–chitosan nanoparticles, which indicates that compounds such as hyaluronic acid increase the release of effective compounds (Fig. 8).

Table 3 Variance analysis of the IC_{50} values of different treatments in the Hs578T and SUM159 cell lines

S.O.V	df	MS	
		Hs578T Cell line	SUM159 Cell line
Treatment	16	327.44**	315.98**
Error	34	4.47	3.63
CV (%)	–	7.81	5.82

** Significance at the one percent probability level

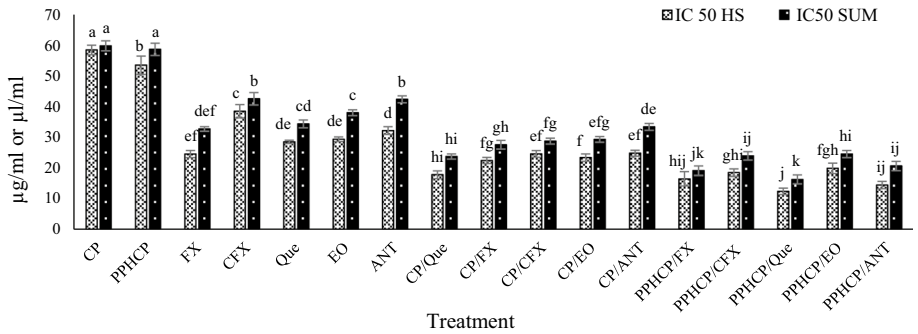

Fig. 9 IC_{50} values of the Hs578T and SUM159 cell lines treated with PLA–chitosan (CP), PLA–PEG–HA/PLA–chitosan (PPHCP), ethanolic extract of *F. vulgare* (FX), ethanolic extract from the selected callus tissue sample (CFX), essential oil of *F. vulgare* (EO), quercetin (Que), anethole (ANT), CP/FX, CP/CFX, CP/EO, CP/Que, CP/ANT, PPHCP/FX, PPHCP/CFX, PPHCP/EO, PPHCP/Que, and PPHCP/ANT

In vitro cytotoxicity

According to the results obtained from the analysis of variance (Table 3), the IC_{50} values of the Hs578T and SUM159 cell lines were significantly ($p < 0.01$) affected by the type of treatment used (FX, CFX, EO, ANT, and Que), the CP and PPHCP nanoparticles, and their combinations.

Investigating the IC_{50} values of the Hs578T and SUM159 cell lines revealed that the Hs578T cell line was more sensitive than the SUM159 cell line at the same concentrations for each treatment (Fig. 9). According to Fig. 9, the treatment of the Hs578T and SUM159 cell lines with the PLA–chitosan and PPHCP nanoparticles had the highest IC_{50} among the different treatments, which indicates that these nanoparticles have the least effect on living organisms and are suitable for the transfer of the mentioned compounds.

On the other hand, the use of PLA–chitosan and PPHCP nanoparticles increased the IC_{50} in both the Hs578T and SUM159 cell lines compared with compounds without nanoparticles (FX), (CFX), (EO), (Que), and (ANT). In addition, the PPHCP nanoparticles had better and more significant effects on reducing the IC_{50} values of the compounds (better effectiveness in drug delivery) than did the PLA–chitosan nanoparticles (Figs. 9, 10).

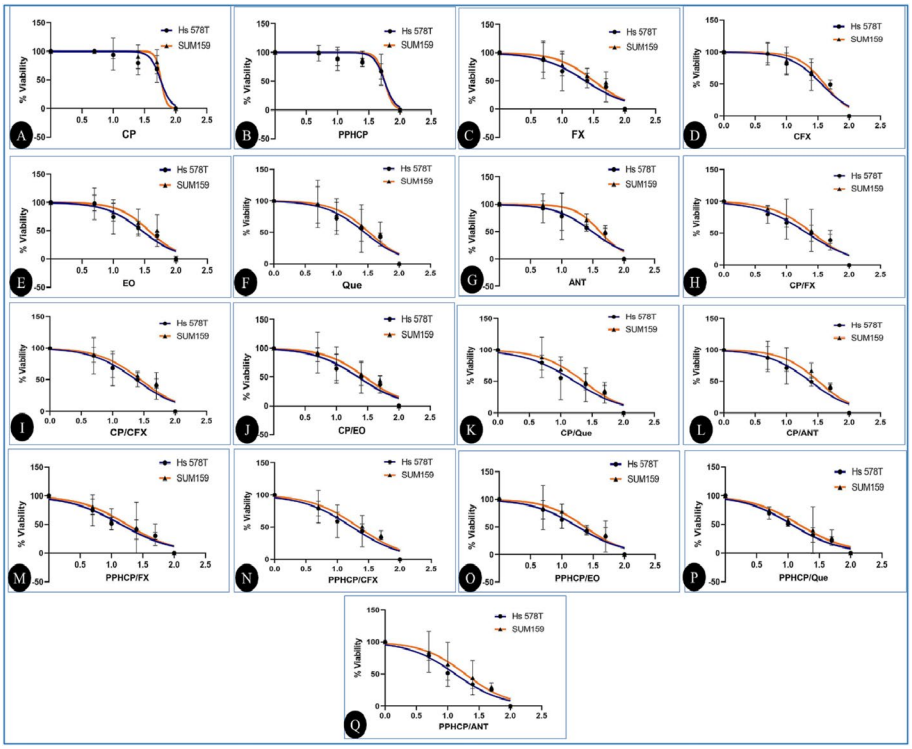

Fig. 10 Evaluation of IC_{50} levels of Hs578T and SUM159 cell lines treated with **A** PLA–chitosan (CP), **B** PLA–PEG–HA/PLA–chitosan (PPHCP), **C** ethanolic extract of *F. vulgare* (FX), **D** ethanolic extract from the selected callus tissue sample (CFX), **E** essential oil of *F. vulgare* (EO), **F** quercetin (Que), **G** anethole (ANT), **H** CP/FX, **I** CP/CFX, **J** CP/EO, **K** CP/Que, **L** CP/ANT, **M** PPHCP/FX, **N** PPHCP/CFX, **O** PPHCP/EO, **P** PPHCP/Que, and **Q** PPHCP/ANT

Table 4 Effects of FX, CFX, EO, ANT, and Que on the percentages of necrotic, pre-apoptotic, and post-apoptotic Hs578T and SUM159 cells

S.O.V	df	MS					
		SUM159 Cell line			Hs578T Cell line		
		Necrotic (%)	Pre-apoptotic (%)	Post-apoptotic (%)	Necrotic (%)	Pre-apoptotic (%)	Post-apoptotic (%)
Treatment	15	0.62**	121.57**	2.77**	4.03**	117.05**	7.89**
Error	32	0.04	3.97	0.14	0.06	0.57	0.06
CV (%)	–	13.07	10.47	7.36	7.09	3.63	4.43

** Significance at the one percent probability level

Cell apoptosis analysis

The analysis of variance of the treatments (FX, CFX, EO, Que, and ANT), CP and PPHCP nanoparticles, and their combinations [(CP/FX), (CP/CFX), (CP/EO), (CP/Que), (CP/ANT), (PPHCP/FX), (PPHCP/CFX), (PPHCP/EO), (PPHCP/Que), and (PPHCP/ANT)] (at the concentrations obtained from the IC_{50} test) in Hs578T and SUM159 revealed that the percentages of necrotic cells and the pre-apoptotic and post-apoptotic stages were significantly ($p < 0.01$) influenced by the type of treatment used (Table 4).

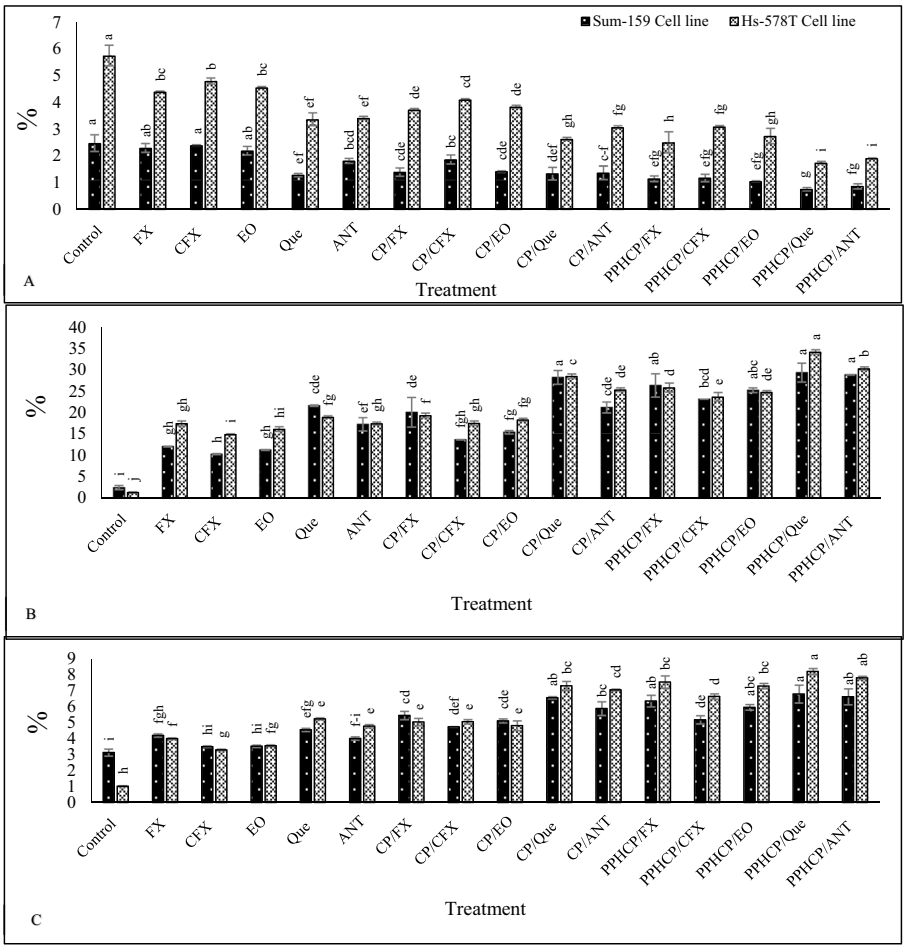

Fig. 11 Effects of PLA–chitosan (CP), PLA–PEG–HA/PLA–chitosan (PPHCP), ethanolic extract of *F. vulgare* (FX), ethanolic extract from the selected callus tissue sample (CFX), essential oil of *F. vulgare* (EO), quercetin (Que), anethole (ANT), CP/FX, CP/CFX, CP/EO, CP/Que, CP/ANT, PPHCP/FX, PPHCP/CFX, PPHCP/EO, PPHCP/Que, and PPHCP/ANT on **A** the percentage of necrotic cells, **B** the pre-apoptotic stage, and **C** the post-apoptotic stage in the Hs578T and SUM159 cell lines

According to the results, in terms of the percentage of necrosis in the SUM159 cell line, no statistically significant difference was observed between most of the treatments. The highest percentage of cell necrosis of the SUM-159 cell line (2.45%) was related to the control cell line (no treatment), and the lowest value (0.74%) was related to the treatment of the same cell line with PPHCP/Que. Moreover, in terms of the percentage of Hs-578T cell line necrosis, a statistically significant difference was observed between the different treatments (Figs. 11, 12A).

In terms of the percentage of Hs578T and SUM159 Hs578T and SUM159 cells in the pre- and post-apoptotic stages treated with the different concentrations, we observed a statistically significant difference overall between the treatments. The highest percentages of cells in the pre- and post-apoptotic stages (34.06% and 8.19%, respectively) nanoparticles, especially nanoparticles containing hyaluronic acid (PPHCP), significantly increased the percentage of Hs578T and SUM159 cells in the pre- and post-apoptotic stages compared with that of free compounds (without nanoparticles).

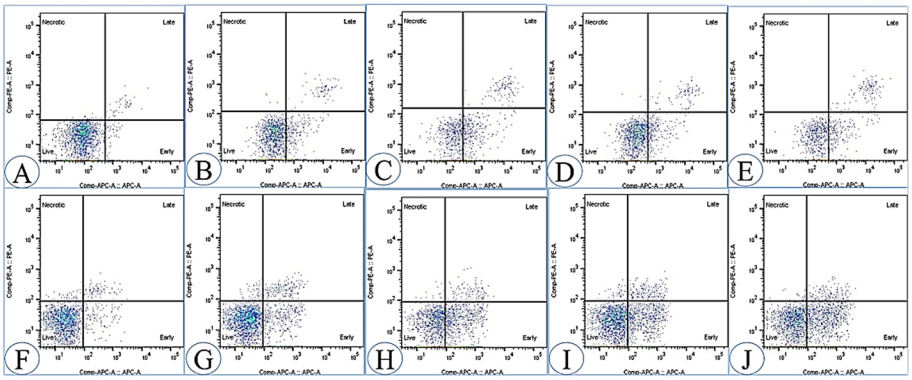

Fig. 12 Flow cytometry data: Hs578T cell line treated; **A** control treatment, **B** FX, **C** Que, **D** PPHCP/FX, and **E** PPHCP/Que; SUM159 cell line treated; **F** control treatment **G** FX, **H** Que, **I** PPHCP/FX, and **J** PPHCP/Que

Discussion

Foeniculum vulgare (Apiaceae) is utilized globally for treating diverse health conditions, such as abdominal pain, arthritis, cancer, constipation, and insomnia (Ghasemian et al. 2020). Phytochemicals such as phenols, alkaloids, terpenoids, flavonoids, glycosides, tannins, and saponins are present in *F. vulgare* methanol extract (Noreen et al. 2023). The main compounds are rutin, quercetin, apigenin, ferulic acid, coumaric acid, and caffeic acid, which have anti-inflammatory and antioxidant properties (Table 2). Additionally, the essential oil extracted from *F. vulgare* seeds has pharmacological effects, such as anti-inflammatory, antispasmodic, and antitumor effects. Chemical analysis revealed that this essential oil contains α-pinene, fenchone, anethole, and estragole (Table 1).

Breast cancer is becoming a growing concern among the female population and significantly influences mortality rates. The use of nanoparticles to transfer herbal medicinal and antioxidant compounds such as quercetin to cancer cells (targeted drug delivery) increases their anticancer potential and reduces their side effects (Lan et al. 2019). Flavonoids inhibit cancer cells through mechanisms such as activating apoptosis, halting the cell cycle, and regulating the expression of various genes, such as those in the Bcl2, Bax, P53, and caspase families, which control tumor growth (Shen et al. 2022). Quercetin acts as an antigrowth drug compound for MCF-7 cells by reducing P38MAPK phosphorylation, which is a prominent sign of cell proliferation (Niazvand et al. 2019). The presence of quercetin in plant compounds affects the G1 phase of tumor cells and causes cell apoptosis by suppressing the expression of cyclin D1, P21, and Twist in SUM159 cells (Hasan et al. 2022). In addition, quercetin has been shown to induce the apoptosis and necrosis of Hs578T cells (Kedhari Sundaram et al. 2019). Quercetin in plant compounds prevents the proliferation of BT-474 cell lines overexpressing the HER2 enzyme by activating the caspase-dependent extrinsic apoptosis stage and suppressing STAT3 signaling (Almatroodi et al. 2021).

In a study conducted by Mohamad et al. (2011), various methods for extracting phytochemical and antioxidant compounds from the ethanolic extract of *F. vulgare* were assessed. They reported that the methanolic extract from the *F. vulgare* aerial part impacted the survival and proliferation of MCF-7 cancer cell lines, showing effectiveness with an acceptable IC_{50} value (Mohamad et al. 2011). Furthermore, our research revealed that the essential oil and ethanol extracts from *F. vulgare* aerial parts effectively

influenced the growth and survival of the Hs578T and SUM159 cell lines. The IC_{50} value observed in the Hs578T cell line treated with extracts from naturally growing samples, as well as essential oil and ethanolic extracts from selected callus samples was lower than that in the Sum-159 cell line, indicating greater resistance of the SUM159 cell line to the medicinal compounds.

In recent years, interest in drug delivery systems utilizing nanoparticles as carriers in the realm of precision medicine for cancer has increased. Nanoparticles, characterized by their solid nature and sizes ranging from 10 to 1000 nm, have emerged as crucial elements in this field (Hetta et al. 2023). The design and synthesis of nanoparticles present two fundamental challenges, namely, the risk of drug nanoparticles accumulating at unintended sites and being misdirected by detrimental agents (Shanmugam et al. 2020).

Owing to their significant utility, polymeric nanoparticles have been utilized in a wide range of fields, such as drug delivery, medical imaging, and early disease detection (Bourang et al. 2024c). The relatively large surface area of polymeric nanoparticles enables easy modification with functional groups, enhancing the specific targeting of drugs in the body (Yao et al. 2020). Moreover, the controlled release characteristics and protective attributes of polymeric nanoparticles render them highly advantageous, particularly in the realm of drug delivery applications (Yanat and Schroën 2021).

Chemotherapy drugs include a variety of agents, such as alkylating agents, antimetabolites, and antitumor antibiotics, as well as compounds from plants and animals with antitumor properties and antitumor hormones (Bourang et al. 2024c). Notably, a significant drawback of chemical drugs is their non-selectivity, while they target tumor cells, they inadvertently harm healthy tissue cells (Dhiman et al. 2021). Polymer nanoparticles serve as an effective solution for addressing these issues encountered in chemotherapy drug administration. These nanoparticles exhibit notable drug-loading ability, enabling efficient drug transport, and the ability to target specific cancerous tissues for drug delivery and regulate the release of drugs (Iqbal et al. 2020). Polymeric nanoparticles have the potential to increase the hydrophilicity of drugs and increase their encapsulation efficiency. This can result in the safeguarding of delicate molecules from degradation and primary metabolism, as well as the extension of drug half-life throughout the metabolic process (Lakshmipriya and Gopinath 2021). According to Fang et al. (2021), dextran-based nanocarriers containing Dox have proven to be a successful method for delivering drugs to treat malignant lymphoma while minimizing cardio-toxic effects. Initially, dextran reacts with a methyl acrylate monomer with the assistance of cerium ammonium nitrate as a catalyst, followed by the addition of a diallyl crosslinking agent (Fang et al. 2021).

Biocompatibility is often described as the property of a particular material to be compatible with a living tissue or organism (Elmowafy et al. 2019). In general, biocompatibility is achieved when the interaction between nanomaterials and the host does not lead to harmful effects such as oxidative stress, DNA damage, mutagenesis, or apoptosis (Islam et al. 2019). Natural polymers such as chitosan, polyethylene glycol, hyaluronic acid, and PCL have high biocompatibility due to their biological origin. Natural polymers offer several benefits, including excellent biocompatibility, controlled enzyme degradation, specific interactions with certain biomolecules, and ease of modification, making them highly adaptable for drug delivery applications (Idrees et al. 2020). These naturally

occurring polymers contain various biological signals, including sequences that promote cell adhesion, allowing them to be recognized by cells. However, their complex structure and chemical composition can lead to variability between batches, affecting outcomes in tissue engineering. The biocompatibility of biomaterials is influenced by both internal factors related to the material itself and external factors tied to the host and implantation site. Internal factors that affect biocompatibility include various parameters such as shape, size, surface chemistry and roughness, design, morphology, porosity, composition, sterility, duration of contact, and degradation. External factors encompass the host species, genetic background, implantation site, and surrounding microenvironment. Together, these factors determine the overall biocompatibility of the implanted material (Elmowafy et al. 2019).

Due to their biocompatibility, PLA and PEG generate non-toxic and safe degradation products, making them ideal for various medical and pharmaceutical applications. The biodegradation process of PLA and PEG-based homopolymers and copolymers involves their hydrolysis into lactic and glycolic acids, which are eventually eliminated from the body as carbon dioxide and water. The biodegradation of PLA and PEG-based drug delivery systems is crucial for regulating the release of loaded drugs (Ramot et al. 2016). As these polymers degrade and erode, the kinetics of drug release depend on both the polymer degradation rate and the diffusion of the drug through the polymer matrix.

On the other hand, the use of biocompatible polymer nanoparticles in large quantities, like other pharmaceutical or non-pharmaceutical compounds in large quantities, is harmful to the body. For example, in targeted drug delivery using polymer nanoparticles, if the amount of chitosan used exceeds the normal or usual amount, there is a possibility of digestive problems (Bor et al. 2016). In addition, when heated, PLA releases an organic compound called VOC. This compound is non-toxic at low concentrations, but some people may experience respiratory irritation or other health effects with prolonged or high exposure.

In this study, PLA–PEG–HA/PLA–chitosan nanoparticles were synthesized successfully to deliver quercetin as a drug, and herbal compounds of *F. vulgare* (Ethanolic extract from aerial part and callus tissues, and essential oil) into SUM159 and Hs578t breast cancer cell lines. For this aim, first, the ethanol extract and essential oil of *F. vulgare* were successfully extracted to assay their anticancer activity in free and encapsulated nanoparticle form in comparison to quercetin.

Dispersion is an important factor in the use of nanoparticles, as the particles can aggregate in samples that show extensive uniformity (Salama et al. 2020). In this research, and according to the results obtained from DLS (Fig. 7A, B), the PLA/chitosan/FX nanoparticles have a peak within a suitable range, which indicates uniformity between the nanoparticles. The size of these nanoparticles was approximately 240 nm. The size and surface charge of nanoparticles are critical factors in the effective delivery of drugs encapsulated within them. Research indicates that reducing the size of nanoparticles enhances their ability to be transported to cancer cells. However, nanoparticles smaller than 50 nm may also lead to increased non-specific absorption by normal cells (Chehelgerdi et al. 2023). This means that while decreasing the size of nanoparticles under 50 nm can improve their transfer efficiency, it also raises the risk of side effects due to greater absorption by healthy cells (Di et al. 2021). The size of these PPHCP/FX

nanoparticles was approximately 350 nm. The presence of a sharp peak in the DLS diagram (Fig. 7B) indicates a uniform structure, which is typically desirable for uniform biological behavior and targeted and predictable drug delivery.

According to the results obtained in this research, the zeta potential values of the PLA–chitosan/FX nanoparticles were positive, and those of the PPHCP/FX nanoparticles were negative (Fig. 7C, D). The negative zeta potential of the nanoparticle may be due to the presence of the hyaluronic acid group in the nanoparticle. A negative zeta potential is an important factor in the stabilization of a nanoparticle suspension. The negative zeta potential causes high repulsive forces in the nanoparticle suspension, which prevents nanoparticle aggregation (Bourang et al. 2024a).

In the research conducted by Noor Alam and colleagues on the development and characterization of PLGA-HA nanoparticles loaded with Cisplatin, a modest increase in the size of nanoparticles conjugated with HA was observed compared to PLGA-only nanoparticles. This increase in size is likely attributed to the incorporation of hyaluronic acid segments. Additionally, the nanoparticles containing HA exhibited a more negative zeta potential, which is attributed to the presence of carboxylic acid groups in hyaluronic acid. Thus, the negative zeta potential observed in these nanoparticles can be linked to the HA content (Alam et al. 2017).

The efficiency of drug encapsulation and release can be affected by various parameters, such as the drug-to-polymer ratio and PVA concentration, when nanoparticles are prepared via the single-solvent emulsion evaporation method (Hammami and Alabdallah 2021). The environment surrounding a tumor is different from that of normal tissue in terms of acidity. The acidity level of tumor tissue is slightly greater than that of healthy tissue (Alipournazari et al. 2024). The energy metabolism of cancer cells is highly dependent on glycolysis, which leads to an increase in the production of lactic acid. Therefore, tumors are more acidic than normal tissues are (Alipournazari et al. 2024). Our results demonstrated that the release rate of medicinal compounds first depends on the pH level and then on the type of encapsulated nanoparticle. According to these results, the possibility of the release of effective compounds and drugs (Que and ANT) from PPHCP nanoparticles was greater than that from PLA–chitosan. Moreover, decreasing the pH from 7.4 to 5 allows for better release of effective compounds (Fig. 8). The enhanced release of Que from PLGA nanoparticles can be explained by the rapid degradation of PLGA under low pH conditions as a pH-responsive polymer (Silva et al. 2022). Similarly, the release of temozolomide-conjugated PLGA nanoparticles loaded with cetuximab at pH = 7.4 and pH = 5.4 was investigated, and it was reported that the optimal drug release from the nanoparticles was found at pH = 5.4 (Senturk et al. 2022). A controlled increase in the release of active compounds and quercetin from PPCPs at acidic pH was observed in our study. Our results revealed that under acidic conditions, PPHCP exhibited a controlled release pattern, and the pH-dependent release of drugs might help improve the efficiency of PPHCP and increase its cytotoxicity.

Bcl-2 protein family members and caspases are key proteins involved in the process of apoptosis (Kaloni et al. 2023). Resistance to apoptosis is one of the main characteristics of cancer cells (Portt et al. 2011). Different studies have shown the effective induction of cell apoptosis by encapsulating active compounds in nanoparticle systems. A study by Sethi et al. (2023) demonstrated that nanoparticles loaded with quercetin stimulated

intrinsic apoptosis more effectively than free quercetin did in liver cancer cells (Sethi et al. 2023), which is consistent with the results obtained in this research (Figs. 11, 12).

The tumor suppressor p53 acts as an upstream inhibitor of NF-kB, a transcription factor located in the nucleus that is responsible for regulating inflammatory reactions (D'Orazi et al. 2021). Increased levels of p53 are believed to potentially suppress NF-kB transcriptional activity. The anethole compound has been demonstrated to be effective at exhibiting anticancer properties by inhibiting cell survival, stimulating apoptosis, and suppressing NF-kB transcriptional activity (Contant et al. 2021). The anticancer and anti-inflammatory effects of anethole may be facilitated through extrinsic and intrinsic initiation of apoptosis, inhibition of cell survival, and suppression of NF-kB signaling.

Conclusion

Copolymer nanoparticles are viewed as a viable option for delivering drugs, essential oils, and plant extracts to address various medical conditions. The findings of the present study suggest that PLA–chitosan and PLA–chitosan–HA copolymer nanoparticles exhibit a strong capacity to target *F. vulgare* plant extracts (aerial parts and selected callus samples), plant essential oils, quercetin, and Anethole compounds specifically toward cancer cells. Nanotechnology-based delivery systems play a significant role in the controlled release of anticancer medications. Progress in the fields of biomaterials and bioengineering has led to the introduction of novel nanoparticle strategies that could revolutionize cancer treatment. The findings of this study indicate that the synthesized copolymer nanoparticles possess the ideal size, dimensions, and zeta potential for efficient transportation and infiltration into the SUM159 and Hs578T triple-negative breast cancer cell lines, thus demonstrating their potential as effective delivery vehicles. Conversely, quercetin and anethole, which are favorable antioxidants that facilitate cellular apoptosis, antitumorigenic activity, and anti-inflammatory properties, can be considered options for further studies in vivo and in vitro.

Abbreviations

^{1}H-NMR	Hydrogen nuclear magnetic resonance spectroscopy
ANT	Trans-anethole
BC	Breast cancer
BSA	Bovine serum albumin
CFX	Ethanolic extract from the designated callus sample
DLS	Dynamic light scattering
DMEM	Dulbecco's modified Eagle's medium
DTG	Thermogravimetric derivative
EE	Retention efficiency
FBS	Fetal bovine serum
FEO	Essential oil of *F. vulgare*
FTIR	Fourier transform infrared spectroscopy
FX	Ethanolic extract of *F. vulgare* plant
GC–MS	Gas chromatography–mass spectrometry
HA	Hyaluronic acid
HPLC	High-performance liquid chromatography
HSA	Human serum albumin
IC_{50}	Half-maximal inhibitory concentration
Kin	Kinetin
MS	Murashige and Skoog culture
NAA	1-Naphthalene acetic acid
NPs	Polymeric nanoparticles
PCL	Poly(ε-caprolactone)
PEG	Polyethylene glycol
PI	Propidium iodide

PLA	Polylactide
PLGA	Poly(DL-lactic-co-glycolic acid)
PVA	Polyvinyl alcohol
Que	Quercetin
SEM	Scanning electron microscopy
SPII	Seed and Plant Improvement Institute
TGA	Thermogravimetric analysis

Acknowledgements
We wish to thank the Vice-Chancellor for Research and Technology of the University of Mohaghegh Ardabili for supporting this work.

Author contributions
M.N and Sh.B conducted the experiments, analyzed the data, and wrote the original draft. S.JG and R.AZ conceived and designed the research, administered and supervised the project, and reviewed and edited the manuscript. Sh.B collaborated in the implementation of HPLC analysis and flow cytometry. S.GR contributed new analytical tools and revised the manuscript. All the authors read and approved the manuscript

Funding
No funding was received for conducting this study.

Data availability
The authors declare that the data supporting the findings of this study are available within the paper and its Supplementary Information files. Should any raw data files be needed in another format, they are available from the corresponding author upon reasonable request.

Declarations

Ethics approval and consent to participate
This article does not contain any studies with human participants or animals performed by any of the authors.

Consent for publication
Not applicable

Competing interests
The authors declare no competing interests.

Received: 30 September 2024 Accepted: 21 March 2025
Published online: 08 April 2025

References

Akbarzadeh I, Shayan M, Bourbour M, Moghtaderi M, Noorbazargan H, Eshrati Yeganeh F, Saffar S, Tahriri M (2021) Preparation, optimization and in-vitro evaluation of curcumin-loaded niosome@ calcium alginate nanocarrier as a new approach for breast cancer treatment. Biology 10(3):173

Akhbari M, Kord R, Jafari Nodooshan S, Hamedi S (2019) Analysis and evaluation of the antimicrobial and anticancer activities of the essential oil isolated from *Foeniculum vulgare* from Hamedan, Iran. Nat Prod Res 33(11):1629–1632

Alam N, Koul M, Mintoo MJ, Khare V, Gupta R, Rawat N, Sharma PR, Singh SK, Mondhe DM, Gupta PN (2017) Development and characterization of hyaluronic acid modified PLGA based nanoparticles for improved efficacy of cisplatin in solid tumor. Biomed Pharmacother 95:856–864

Alipournazari P, Pourmadadi M, Abdouss M, Rahdar A, Pandey S (2024) Enhanced delivery of doxorubicin for breast cancer treatment using pH-sensitive starch/PVA/g-C3N4 hydrogel. Int J Biol Macromol 265:130901

Almatroodi SA, Alsahli MA, Almatroudi A, Verma AK, Aloliqi A, Allemailem KS, Khan AA, Rahmani AH (2021) Potential therapeutic targets of quercetin, a plant flavonol, and its role in the therapy of various types of cancer through the modulation of various cell signaling pathways. Molecules 26(5):1315

Al-Nemrawi N, Hameedat F, Al-Husein B, Nimrawi S (2022) Photolytic controlled release formulation of methotrexate loaded in chitosan/TiO2 nanoparticles for breast cancer. Pharmaceuticals 15(2):149

Alrushaid N, Khan FA, Al-Suhaimi EA, Elaissari A (2023) Nanotechnology in cancer diagnosis and treatment. Pharmaceutics 15(3):1025

Arnold M, Morgan E, Rumgay H, Mafra A, Singh D, Laversanne M, Vignat J, Gralow JR, Cardoso F, Siesling S (2022) Current and future burden of breast cancer: Global statistics for 2020 and 2040. Breast 66:15–23

Bai J, Zheng Y, Wang G, Liu P (2016) Protective effect of D-limonene against oxidative stress-induced cell damage in human lens epithelial cells via the p38 pathway. Oxid Med Cell Longev 2016:5962832

Bettaieb I, Bourgou S, Sriti J, Msaada K, Limam F, Marzouk B (2011) Essential oils and fatty acids composition of Tunisian and Indian cumin (*Cuminum cyminum* L.) seeds: a comparative study. J Sci Food Agric 91(11):2100–2107

Bholakant R, Dong B, Zhou X, Huang X, Zhao C, Huang D, Zhong Y, Qian H, Chen W, Feijen J (2021) Multi-functional polymeric micelles for chemotherapy-based combined cancer therapy. J Mater Chem B 9(42):8718–8738

Boevé J-L, Sonet G, Jacobson HR, Angeli S (2023) Cypress terpenes in sawfly larva of *Susana cupressi* (Hymenoptera: Symphyta: Tenthredinoidea). Sci Nat 110(2):13

Bor G, Mytych J, Zebrowski J, Wnuk M, Şanlı-Mohamed G (2016) Cytotoxic and cytostatic side effects of chitosan nanoparticles as a non-viral gene carrier. Int J Pharm 513(1–2):431–437
Bourang S, Asadian S, Noruzpour M, Mansuryar A, Azizi S, Ebrahimi HA, Amani Hooshyar V (2024a) PLA-HA/Fe_3O_4 magnetic nanoparticles loaded with curcumin: physicochemical characterization and toxicity evaluation in HCT116 colorectal cancer cells. Discover Appl Sci 6(4):186
Bourang S, Jahanbakhsh S, Asghari Zakariya R, Parsa-Khankandi H, Noruzpuor M (2024b) The effect of different Elicitors on the amount of biochemical compounds and some secondary metabolites of callus tissue of fennel (*Foeniculum vulgare*). Iran J Rangelands Forests Plant Breed Genetic Res. https://doi.org/10.22092/IJRFPBGR.2024.363423.1449
Bourang Sh, Noruzpour M, Jahanbakhsh Godekahriz S, Ebrahimi HAC, Amani A, Asghari Zakaria R, Yaghoubi H. Application of nanoparticles in breast cancer treatment: a systematic review. Naunyn-Schmiedeberg's Archives of Pharmacology. 2024:1-47.
Calahorra J, Blaya-Cánovas JL, Castellini-Pérez O, Aparicio-Puerta E, Cives-Losada C, Marin JJ, Rementeria M, Cara FE, López-Tejada A, Griñán-Lisón C (2024) Unlocking the effective alliance of β-lapachone and hydroxytyrosol against triple-negative breast cancer cells. Biomed Pharmacother 174:116439
Chainy GB, Manna SK, Chaturvedi MM, Aggarwal BB (2000) Anethole blocks both early and late cellular responses transduced by tumor necrosis factor: effect on NF-κB, AP-1, JNK, MAPKK and apoptosis. Oncogene 19(25):2943–2950
Chandrasekhar SN, Mallikarjun SB, Salim HP (2020) Comparative evaluation of antibacterial activity of probiotics SK12 and SM18: an in vitro study. Int J Clin Pediatr Dent 13(6):611
Chehelgerdi M, Chehelgerdi M, Allela OQB, Pecho RDC, Jayasankar N, Rao DP, Thamaraikani T, Vasanthan M, Viktor P, Lakshmaiya N (2023) Progressing nanotechnology to improve targeted cancer treatment: overcoming hurdles in its clinical implementation. Mol Cancer 22(1):169
Contant C, Rouabhia M, Loubaki L, Chandad F, Semlali A (2021) Anethole induces anti-oral cancer activity by triggering apoptosis, autophagy and oxidative stress and by modulation of multiple signaling pathways. Sci Rep 11(1):13087
Correia AS, Gärtner F, Vale N (2021) Drug combination and repurposing for cancer therapy: the example of breast cancer. Heliyon. 7(1):e05948
D'Orazi G, Cordani M, Cirone M (2021) Oncogenic pathways activated by pro-inflammatory cytokines promote mutant p53 stability: clue for novel anticancer therapies. Cell Mol Life Sci 78(5):1853–1860
da Silva FF, Agner T, Sayer C, Lona LMF (2022) Curcumin encapsulation in functional PLGA nanoparticles: a promising strategy for cancer therapies. Adv Coll Interf Sci 300:102582
Das A, Ghosh S, Pramanik N (2024) Chitosan biopolymer and its composites: processing, properties and applications—a comprehensive review. Hybrid Adv 6:100265
Dávila-González D, Choi DS, Rosato RR, Granados-Principal SM, Kuhn JG, Li W-F, Qian W, Chen W, Kozielski AJ, Wong H (2018) Pharmacological inhibition of NOS activates ASK1/JNK pathway augmenting docetaxel-mediated apoptosis in triple-negative breast cancer. Clin Cancer Res 24(5):1152–1162
Della Sala F, Fabozzi A, di Gennaro M, Nuzzo S, Makvandi P, Solimando N, Pagliuca M, Borzacchiello A (2022) Advances in hyaluronic-acid-based (nano) devices for cancer therapy. Macromol Biosci 22(1):2100304
Dhiman N, Awasthi R, Sharma B, Kharkwal H, Kulkarni GT (2021) Lipid nanoparticles as carriers for bioactive delivery. Front Chem 9:580118
Di J, Gao X, Du Y, Zhang H, Gao J, Zheng A (2021) Size, shape, charge and "stealthy" surface: carrier properties affect the drug circulation time in vivo. Asian J Pharm Sci 16(4):444–458
Elmowafy EM, Tiboni M, Soliman ME (2019) Biocompatibility, biodegradation and biomedical applications of poly (lactic acid)/poly (lactic-co-glycolic acid) micro and nanoparticles. J Pharm Investig 49:347–380
Esmeeta A, Adhikary S, Dharshnaa V, Swarnamughi P, Maqsummiya ZU, Banerjee A, Pathak S, Duttaroy AK (2022) Plant-derived bioactive compounds in colon cancer treatment: an updated review. Biomed Pharmacother 153:113384
Fang K, Wang L, Huang H, Dong S, Guo Y (2021) Therapeutic efficacy and cardioprotection of nucleolin-targeted doxorubicin-loaded ultrasound nanobubbles in treating triple-negative breast cancer. Nanotechnology 32(24):245102
Farkas N-I, Marincaș L, Barabás R, Bizo L, Ilea A, Turdean GL, Toșa M, Cadar O, Barbu-Tudoran L (2022) Preparation and characterization of doxycycline-loaded electrospun PLA/HAP nanofibers as a drug delivery system. Materials 15(6):2105
Ghasemian A, Al-Marzoqi A-H, Mostafavi SKS, Alghanimi YK, Teimouri M (2020) Chemical composition and antimicrobial and cytotoxic activities of *Foeniculum vulgare* Mill essential oils. J Gastroint Cancer. 51:260–266
Gregoriou Y, Gregoriou G, Yilmaz V, Kapnisis K, Prokopi M, Anayiotos A, Strati K, Dietis N, Constantinou AI, Andreou C (2021) Resveratrol loaded polymeric micelles for theranostic targeting of breast cancer cells. Nanotheranostics. 5(1):113
Hammami I, Alabdallah NM (2021) Gold nanoparticles: synthesis properties and applications. J King Saud Univ Sci 33(7):101560
Hasan AA, Tatarskiy V, Kalinina E (2022) Synthetic pathways and the therapeutic potential of quercetin and curcumin. Int J Mol Sci 23(22):14413
Herdiana Y, Wathoni N, Shamsuddin S, Joni IM, Muchtaridi M (2021) Chitosan-based nanoparticles of targeted drug delivery system in breast cancer treatment. Polymers 13(11):1717
Hetta HF, Ramadan YN, Al-Harbi AI, A. Ahmed E, Battah B, Abd Ellah NH, Zanetti S, Donadu MG (2023) Nanotechnology as a promising approach to combat multidrug resistant bacteria: a comprehensive review and future perspectives. Biomedicines. 11(2):413
Hurst WJ, Snyder KP, Martin RA Jr (1983) The determination of iodine in milk and milk chocolate by anion HPLC. J Liq Chromatogr 6(11):2067–2077
Ibrahim M, Abuwatfa WH, Awad NS, Sabouni R, Husseini GA (2022a) Encapsulation, release, and cytotoxicity of doxorubicin loaded in liposomes, micelles, and metal-organic frameworks: a review. Pharmaceutics 14(2):254
Ibrahim M, Ramadan E, Elsadek NE, Emam SE, Shimizu T, Ando H, Ishima Y, Elgarhy OH, Sarhan HA, Hussein AK (2022b) Polyethylene glycol (PEG): the nature, immunogenicity, and role in the hypersensitivity of PEGylated products. J Controll Release. 351:215–230
Idrees H, Zaidi SZJ, Sabir A, Khan RU, Zhang X, Hassan SU (2020) A review of biodegradable natural polymer-based nanoparticles for drug delivery applications. Nanomaterials 10(10):1970

Ioele G, Chieffallo M, Occhiuzzi MA, De Luca M, Garofalo A, Ragno G, Grande F (2022) Anticancer drugs: recent strategies to improve stability profile, pharmacokinetic and pharmacodynamic properties. Molecules 27(17):5436
Iqbal S, Qu Y, Dong Z, Zhao J, Khan AR, Rehman S, Zhao Z (2020) Poly (β-amino esters) based potential drug delivery and targeting polymer; an overview and perspectives. Eur Polym J 141:110097
Islam N, Dmour I, Taha MO (2019) Degradability of chitosan micro/nanoparticles for pulmonary drug delivery. Heliyon. 5(5):e01684
Jin H, Pi J, Zhao Y, Jiang J, Li T, Zeng X, Yang P, Evans CE, Cai J (2017) EGFR-targeting PLGA-PEG nanoparticles as a curcumin delivery system for breast cancer therapy. Nanoscale 9(42):16365–16374
Junnuthula V, Kolimi P, Nyavanandi D, Sampathi S, Vora LK, Dyawanapelly S (2022) Polymeric micelles for breast cancer therapy: recent updates, clinical translation and regulatory considerations. Pharmaceutics 14(9):1860
Kalaydina R-V, Bajwa K, Qorri B, Decarlo A, Szewczuk MR (2018) Recent advances in "smart" delivery systems for extended drug release in cancer therapy. Int J Nanomed 13:4727–4745
Kaloni D, Diepstraten ST, Strasser A, Kelly GL (2023) BCL-2 protein family: attractive targets for cancer therapy. Apoptosis 28(1):20–38
Kang G, Mishyna M, Appiah KS, Yamada M, Takano A, Prokhorov V, Fujii Y (2019) Screening for plant volatile emissions with allelopathic activity and the identification of L-Fenchone and 1, 8-Cineole from star anise (*Illicium verum*) leaves. Plants 8(11):457
Kaur B, Rolta R, Salaria D, Kumar B, Fadare OA, da Costa RA, Ahmad A, Al-Rawi MBA, Raish M, Rather IA (2022) An in silico investigation to explore anti-cancer potential of *Foeniculum vulgare* Mill. Phytoconstituents for the management of human breast cancer. Molecules 27(13):4077
Kedhari Sundaram M, Raina R, Afroze N, Bajbouj K, Hamad M, Haque S, Hussain A (2019) Quercetin modulates signaling pathways and induces apoptosis in cervical cancer cells. Biosci Rep 39(8):BSR20190720
Khosraviboroujeni A, Mirdamadian SZ, Minaiyan M, Taheri A (2022) Preparation and characterization of 3D printed PLA microneedle arrays for prolonged transdermal drug delivery of estradiol valerate. Drug Deliv Transl Res 12(5):1195–1208
Kiani-Dehkordi B, Vatanara A, Amini M, Hamidi M, Dibaei M, Norouzi P, Rezaei S, Khoshnazar A, Rouini M (2023) Preparation of polymersomes from synthesized hyaluronic acid-graft-poly (ε-caprolactone) copolymers for drug delivery to the brain. Mater Today Chem 30:101504
Lakshmipriya T, Gopinath SC (2021) Introduction to nanoparticles and analytical devices. Nanoparticles in analytical and medical devices. Elsevier, Amsterdam, pp 1–29
Lan C-Y, Chen S-Y, Kuo C-W, Lu C-C, Yen G-C (2019) Quercetin facilitates cell death and chemosensitivity through RAGE/PI3K/AKT/mTOR axis in human pancreatic cancer cells. J Food Drug Analy 27(4):887–896
Levit SL, Tang C (2021) Polymeric nanoparticle delivery of combination therapy with synergistic effects in ovarian cancer. Nanomaterials 11(4):1048
Lima AL, Alves AF, Xavier AL, Mozzini-Monteiro T, Oliveira TR, Leite FC, Matias WN, Branco MV, Souza MF, Piuvezam MR (2016) Anti-inflammatory activity and acute toxicity studies of hydroalcoholic extract of Herissantia tiubae. Rev Bras Farmacogn 26:225–232
Lutviani S, Anisa IN, Soemardji AA (2023) Anti-inflammatory and mucolytic activity test of ethanol extract fennel leaf (*Foeniculum vulgare* Mill.). In: Sukweenadhi J, Setiawan F (eds) Conference on natural resources and life sciences 2022 (NRLS-BIO 2022). Atlantis Press, Dordrecht
Mirzaei S, Gholami MH, Ang HL, Hashemi F, Zarrabi A, Zabolian A, Hushmandi K, Delfi M, Khan H, Ashrafizadeh M (2021) Pre-clinical and clinical applications of small interfering RNAs (siRNA) and co-delivery systems for pancreatic cancer therapy. Cells 10(12):3348
Mohamad RH, El-Bastawesy AM, Abdel-Monem MG, Noor AM, Al-Mehdar HAR, Sharawy SM, El-Merzabani MM (2011) Antioxidant and anticarcinogenic effects of methanolic extract and volatile oil of fennel seeds (*Foeniculum vulgare*). J Med Food 14(9):986–1001
Mosleh-Shirazi S, Abbasi M, Reza Moaddeli M, Vaez A, Shafiee M, Kasaee SR, Amani AM, Hatam S (2022) Nanotechnology advances in the detection and treatment of cancer: an overview. Nanotheranostics. 6(4):400
Mundel R, Thakur T, Chatterjee M (2022) Emerging uses of PLA–PEG copolymer in cancer drug delivery. 3 Biotech. 12(2):41
Nasır A, Yabalak E (2021) Investigation of antioxidant, antibacterial, antiviral, chemical composition, and traditional medicinal properties of the extracts and essential oils of the Pimpinella species from a broad perspective: a review. J Essent Oil Res 33(5):411–426
Nguyen DT, Nguyen N-M, Vu D-M, Tran M-D, Ta V-T (2021) On-demand release of drug from magnetic nanoparticle-loaded alginate beads. J Analyt Methods Chem. 2021(1):5576283
Niazvand F, Orazizadeh M, Khorsandi L, Abbaspour M, Mansouri E, Khodadadi A (2019) Effects of quercetin-loaded nanoparticles on MCF-7 human breast cancer cells. Medicina 55(4):114
Noreen S, Tufail T, Badar Ul Ain H, Awuchi CG (2023) Pharmacological, nutraceutical, functional and therapeutic properties of fennel (*Foeniculum vulgare*). Int J Food Prop 26(1):915–927
Organization WHO. Breast cancer 2024. https://www.who.int/news-room/fact-sheets/detail/breast-cancer. Accessed 13 Mar 2024
Parveen S, Sahoo SK (2011) Long circulating chitosan/PEG blended PLGA nanoparticle for tumor drug delivery. Eur J Pharmacol 670(2–3):372–383
Pomeroy AE, Schmidt EV, Sorger PK, Palmer AC (2022) Drug independence and the curability of cancer by combination chemotherapy. Trends Cancer. 8(11):915–929
Portt L, Norman G, Clapp C, Greenwood M, Greenwood MT (2011) Anti-apoptosis and cell survival: a review. Biochim Biophys Acta Mol Cell Res 1813(1):238–259
Prajapati RN, Bhushan B, Singh K, Chopra H, Kumar S, Agrawal M, Pathak D, Chanchal DK, Laxmikant (2024) Recent advances in pharmaceutical design: unleashing the potential of novel therapeutics. Curr Pharm Biotechnol 25(16):2060–2077

Qiu X, Qu Y, Guo B, Zheng H, Meng F, Zhong Z (2022) Micellar paclitaxel boosts ICD and chemo-immunotherapy of metastatic triple negative breast cancer. J Controll Release. 341:498–510
Ramot Y, Haim-Zada M, Domb AJ, Nyska A (2016) Biocompatibility and safety of PLA and its copolymers. Adv Drug Deliv Rev 107:153–162
Rather RA, Bhagat M (2020) Quercetin as an innovative therapeutic tool for cancer chemoprevention: Molecular mechanisms and implications in human health. Cancer Med 9(24):9181–9192
Rauf A, Ahmad F, Sehar S, Khawaja AA, Haroon SM, Iqbal R (2022) A concise review on toxicity and pharmacological aspects of *Foeniculum vulgare* with emphasis on anti-cancer potential. Indian J. https://doi.org/10.52711/2231-5659.2022.00013
Reyes-Farias M, Carrasco-Pozo C (2019) The anti-cancer effect of quercetin: molecular implications in cancer metabolism. Int J Mol Sci 20(13):3177
Rios de la Rosa JM, Tirella A, Tirelli N (2018) Receptor-Targeted drug delivery and the (many) problems we know of: the case of CD44 and hyaluronic acid. Adv Biosyst 2(6):1800049
Roy A, Park H-J, Jung HA, Choi JS (2018) Estragole exhibits anti-inflammatory activity with the regulation of NF-κB and Nrf-2 signaling pathways in LPS-induced RAW 264.7 cells. Nat Prod Sci 24(1):13–20
Saghaeidehkordi A (2021) Development of novel peptide-doxorubicin conjugates for targeting triple-negative breast cancer. Chapman University
Salama AH, Abdelkhalek AA, Elkasabgy NA (2020) Etoricoxib-loaded bio-adhesive hybridized polylactic acid-based nanoparticles as an intra-articular injection for the treatment of osteoarthritis. Int J Pharm 578:119081
Senturk F, Cakmak S, Gumusderelioglu M, Ozturk GG (2022) Hydrolytic instability and low-loading levels of temozolomide to magnetic PLGA nanoparticles remain challenging against glioblastoma therapy. J Drug Deliv Sci Technol 68:103101
Sethi G, Rath P, Chauhan A, Ranjan A, Choudhary R, Ramniwas S, Sak K, Aggarwal D, Rani I, Tuli HS (2023) Apoptotic mechanisms of quercetin in liver cancer: recent trends and advancements. Pharmaceutics 15(2):712
Shah A, Aftab S, Nisar J, Ashiq MN, Iftikhar FJ (2021) Nanocarriers for targeted drug delivery. J Drug Deliv Sci Technol. 62:102426
Shanmugam S, Hari A, Pandey A, Mathimani T, Felix L, Pugazhendhi A (2020) Comprehensive review on the application of inorganic and organic nanoparticles for enhancing biohydrogen production. Fuel 270:117453
Shen N, Wang T, Gan Q, Liu S, Wang L, Jin B (2022) Plant flavonoids: classification, distribution, biosynthesis, and antioxidant activity. Food Chem 383:132531
Shi L, Zhang J, Zhao M, Tang S, Cheng X, Zhang W, Li W, Liu X, Peng H, Wang Q (2021) Effects of polyethylene glycol on the surface of nanoparticles for targeted drug delivery. Nanoscale 13(24):10748–10764
Shu H, Zhang W, Yun Y, Chen W, Zhong Q, Hu Y, Chen H, Chen W (2020) Metabolomics study on revealing the inhibition and metabolic dysregulation in *Pseudomonas fluorescens* induced by 3-carene. Food Chem 329:127220
Smolarz B, Nowak AZ, Romanowicz H (2022) Breast cancer—epidemiology, classification, pathogenesis and treatment (review of literature). Cancers 14(10):2569
Tang L, Chen M, Wang D, He Y, Ge G, Zeng Z, Shu J, Guo W, Wu SX, Xiong W (2024) Doxorubicin and iron-doped mesoporous silica nanoparticles for chemodynamic therapy and chemotherapy of breast cancer. N J Chem 48(39):17294–17309
Tedeschini T, Campara B, Grigoletto A, Bellini M, Salvalaio M, Matsuno Y, Suzuki A, Yoshioka H, Pasut G (2021) Polyethylene glycol-based linkers as hydrophilicity reservoir for antibody-drug conjugates. J Controll Release. 337:431–447
Tian B, Liu J (2023) Smart stimuli-responsive chitosan hydrogel for drug delivery: a review. Int J Biol Macromol 235:123902
Verma VS, Pandey A, Jha AK, Badwaik HKR, Alexander A, Ajazuddin, (2024) Polyethylene glycol–based polymer-drug conjugates: novel design and synthesis strategies for enhanced therapeutic efficacy and targeted drug delivery. Appl Biochem Biotechnol. https://doi.org/10.1007/s12010-024-04895-6
Wangchuk P (2018) Therapeutic applications of natural products in herbal medicines, biodiscovery programs, and biomedicine. J Biol Active Prod Nat 8(1):1–20
Yanat M, Schroën K (2021) Preparation methods and applications of chitosan nanoparticles; with an outlook toward reinforcement of biodegradable packaging. React Funct Polym 161:104849
Yang J, Shi Z, Liu R, Wu Y, Zhang X (2020) Combined-therapeutic strategies synergistically potentiate glioblastoma multiforme treatment via nanotechnology. Theranostics. 10(7):3223
Yao Y, Zhou Y, Liu L, Xu Y, Chen Q, Wang Y, Wu S, Deng Y, Zhang J, Shao A (2020) Nanoparticle-based drug delivery in cancer therapy and its role in overcoming drug resistance. Front Mol Biosci 7:193
Zhang Y, Yue S, Haag R, Sun H, Zhong Z (2021) An intelligent cell-selective polymersome-DM1 nanotoxin toward triple negative breast cancer. J Controll Release. 340:331–341

Publisher's Note